

## Supplemental Material for

Chavez et al.,

### SUMOYLATION AND THE STRUCTURAL MAINTENANCE OF CHROMOSOMES (SMC) 5/6 COMPLEX SLOW SENESCENCE THROUGH RECOMBINATION INTERMEDIATE RESOLUTION.

#### Supplemental Materials and Methods:

**Spot assays:** Yeast were grown in YPAD overnight at 23°C, pelleted and resuspended into 1x PBS and counted. Equal numbers of cells were then serially diluted either 5-fold or 10-fold and spotted onto plates containing YPAD or YPAD containing MMS or HU. The plates were then incubated at 30°C (unless otherwise noted) and photographed 2-3 days later.

**UBA2 manipulation:** For the experiment comparing senescence in *tlc1Δ UBA2* versus *tlc1Δ uba2-ts10*, a *cir<sup>0</sup> TLC1/tlc1Δ UBA2/uba2Δ* diploid (YAC24; Supplementary Table 3) was transformed with either the WT or temperature sensitive *UBA2* allele on a pRS416 plasmid backbone. Each diploid was then sporulated and the senescence of *tlc1Δ uba2Δ* haploids carrying either plasmid were compared. Importantly, the derived haploid cells that were *tlc1Δ* but contained the endogenous *UBA2* allele senesced at a comparable PD between the two different diploids, indicating that both diploids had comparable telomere lengths, before the assay began (data not shown). Other experiments involving manipulations of the E1 sumo-ligase *UBA2* were performed utilizing plasmid-based complementation with either a *UBA2* or *uba2-ts10* allele within a *uba2Δ* background. For simplicity these strains are referred to as *UBA2* or *uba2-ts10* respectively.

**Candidate sumoylated protein screen:** The TAP-tagged *S. cerevisiae* BY4741 library (Open Biosystems), (1), was used to identify novel proteins subject to sumoylation, and to determine the E3 ligases responsible. Duplicates of each strain were grown to log phase and one sample from each set was treated with 0.3% MMS. Both samples were then incubated for an additional 2

hours at 30°C. Cells were collected and resuspended into TE supplemented with 10 mM N-ethyl maleimide (NEM), placed on ice for 5 min., pelleted, and flash frozen in liquid N<sub>2</sub>. Proteins were extracted using trichloroacetic acid, separated by SDS-PAGE, and immunoblots were probed with anti-TAP antibodies (Open Biosystems #cab1001, used at a 1:800 dilution). Proteins that showed possible sumoylation were verified using a modified SUMO-finger print method (2). Briefly, YAC357 was crossed to the desired TAP strain, sporulated and haploids were generated that carried a plasmid expressing a *YFP-SMT3* fusion gene as their sole source of *SMT3*. The pattern of sumoylation between the wildtype (*SMT3*) and fusion (*YFP-SMT3*) TAP expressing strains were then compared. If bands seen in *SMT3* expressing cells were due to sumoylation then a shift in their migration to higher mobility species was seen in *YFP-SMT3* expressing cells. Predictions of the number of SUMO molecules added to target substrates were also obtained from the sumo-finger print method and are listed in Supplementary Table 2. To determine the E3 ligase responsible for sumoylation, strains YAC317, 389-393 were crossed to the desired TAP-expressing clone, sporulated and haploids with the desired genotype were selected and tested.

### **Supplemental Figures Legends**

**Supplemental Figure 1:** Senescence curve performed at 30°C, comparing the rates of senescence of *tlc1Δ UBA2* and *tlc1Δ uba2-ts10* cells. Telomerase positive controls are shown.

**Supplemental Figure 2:** Senescence curve, comparing the senescence rates of *tlc1Δ* cells with the indicated different single SUMO E3 ligase mutations. Telomerase positive controls are shown.

**Supplemental Figure 3:** Senescence curve, comparing the senescence rates of *tlc1Δ* cells with the indicated different double combinations of SUMO E3 ligase mutations. Telomerase positive controls are shown.

**Supplemental Figure 4:** SUMO deficiency does not rescue the slow growth of *top3Δ* cells.

Spot assay comparing the relative growth rates of strains at 30°C. All strains are *uba2Δ* and are transformed with a plasmid containing either *UBA2* or the *uba2-ts10* allele. Large single colonies on a lawn of small colonies most likely represent the occurrence of suppressor mutations that are known to occur spontaneously at high frequency in *top3Δ* strains.

**Supplemental Figure 5:** Description of 2DGE and the Y'-Long probe. (A) Migration pattern of various DNA species within 2D gels. First dimension migration in low percentage agarose and low voltage separates DNA molecules mainly by size, and second dimension migration in high percentage agarose plus ethidium bromide and high voltage separates DNA molecules mainly by shape. The dotted lime-green line traces over the region of the replication arc (RA) and X-spike (XS). The pink diagrams depict the various structures that run at each region on the RA and XS. (B) An example of the structure of an *S. cerevisiae* telomere showing Y'-Short and Y'-Long elements and demonstrating the difference in fragment length between internal and terminal Y'-Long elements. Due to the existence of two distinct Y'-Long elements (internal and terminal) analysis of replication intermediates using the Y'-Long probe leads two distinct replication arcs and X-spikes being visualized during 2D gel analysis. (C) The migration pattern of the RA and X-shaped molecules corresponding to the internal (I) and terminal (T) Y'-Long elements within 2D gels are shown. The location of a hybrid "H" X-spike is also indicated. This spike is accentuated in Smc5/6 complex mutants and we hypothesize that it represents a physical linkage between a terminal and an internal Y'-Long element that have undergone a recombination event (Supplemental Fig. 14), although additional inappropriate linkages are possible and further described in Supplemental Fig. 15.

**Supplemental Figure 6:** Siz1 and Siz2 do not regulate the level of telomere recombination intermediates during senescence. (A) Representative 2D-gel analysis of replication intermediates accumulated in *tlc1Δ* and *tlc1Δ siz1Δ siz2Δ* strains at the telomere visualized with a probe specific for Y'-Long elements. (B) Comparisons of the ratio of X-shaped molecules to the replication arc within the telomere in *tlc1Δ* and *tlc1Δ siz1Δ siz2Δ* mutants at 53 PD after spore germination. Data represents the mean and standard error of four independent samples per genotype.

**Supplemental Figure 7:** Mms21 and Smc6 affect the level of telomere X-structures in the absence, but not presence, of telomerase. (A) Representative 2D-gel analysis of telomere replication intermediates (visualized with a probe specific for Y'-Long elements) in WT, *mms21-sp* and *smc6-9* mutants. (B) Comparisons of the ratio of X-shaped molecules to the replication arc within the telomere in WT, *mms21-sp* and *smc6-9* mutants. Data represents the mean and standard error of two or three independent samples per genotype.

**Supplemental Figure 8:** Mms21 does not support Ku-dependent telomere capping. Yku70 and a second protein Cdc13 cooperate to cap telomere ends, and *yku70Δ cdc13-1* mutants lose capping function at 25°C, a temperature permissive to the growth of either single mutant (3,4). However, *mms21-sp* did not affect the growth of *cdc13-1* mutants at temperatures ranging from 25°C to 37°C, indicating that telomere capping by Yku70 is independent of Mms21-dependent sumoylation. (A) Spot assay comparing the growth of various *mms21-sp*, *cdc13-1* and *yku70Δ* mutants. No increase in temperature sensitive growth was seen in any of the analyzed double mutants (there is a slight decrease in growth even at permissive temperatures due to the slow growth phenotype conferred by the *mms21-sp* mutation). (B) Spot assay comparing the growth rate of *mms21-sp* and *cdc13-1* single and double mutants utilizing a more moderate temperature increase (to 27°C). No increase in temperature sensitive growth was observed. In addition,

senescence analysis was attempted to test if the rapid senescence of *tlc1Δ mms21-sp* mutants is epistatic with *yku70Δ* mutation. However, the rapid senescence rate of *tlc1Δ yku70Δ* mutants (which doubled fewer than 25 times after sporulation) precluded a quantitative determination of any possible contribution of Mms21 to Yku70 function during senescence (data not shown). However we did observe that *tlc1Δ yku70Δ* cells formed survivors more readily than *tlc1Δ yku70Δ mms21-sp* cells, suggesting that Mms21 has Yku70-independent effects that impact telomere maintenance, and further arguing that Yku70 is not a key target of Mms21 in telomere maintenance (data not shown).

**Supplemental Figure 9:** Spot assay performed at 30°C comparing the relative growth rates of Smc5/6 complex mutants in the indicated media.

**Supplemental Figure 10:** Senescence curves, comparing the senescence rates of *tlc1Δ smc5-6* and *tlc1Δ smc6-9* mutants versus *tlc1Δ* controls, shown in panels A and B, respectively. Telomerase positive controls are shown.

**Supplemental Figure 11:** Deletion of *SIZ1* or *SIZ2* does not grossly affect the growth rate of *smc5-6* or *smc6-9* mutants. Strains were grown at 30°C on YPAD.

**Supplemental Figure 12:** Smc5 sumoylation increases during senescence, and the increase is dependent upon Mms21. (A) *tlc1Δ* strains expressing a TAP tagged form of Smc5 were senesced and the levels of sumoylated Smc5 were determined between early and late senescent cells. The ratio of sumoylated Smc5 to total Smc5 is shown below each lane. (B) A similar experiment as in panel A is shown except that *tlc1Δ mms21-sp* mutants expressing TAP tagged Smc5 were used.

**Supplemental Figure 13:** Smc5 prevents the accumulation of X-structures during senescence.

(A) Representative 2D-gel analysis of replication intermediates accumulated in *tlc1Δ* and *tlc1Δ smc5-31* strains at the telomere visualized with a Y'-Long specific probe. (B) Comparisons of the ratio of X-shaped molecules to the replication arc within the telomere for *tlc1Δ* and *tlc1Δ smc5-31* cells at 45 PD after spore germination. The means and standard errors from four independent samples per genotype are shown. Because the *smc5-31* allele is plasmid-based and is a recessive allele ((5) and unpublished observations), these particular 2D gels were done by sporulating diploid cells heterozygous for wild type and deletion alleles each of *TLC1* and *SMC5* and containing the *smc5-31* plasmid based allele [pGC251-*LEU2 smc5-31*]. Germinated *tlc1Δ* mutants that maintained [pGC251-*LEU2 smc5-31*] but contained a wild-type genomic copy of the *SMC5* were used as controls for the *tlc1Δ smc5Δ* [pGC251-*LEU2 smc5-31*] mutant cells. All samples for this experiment were grown in selective media to assure plasmid maintenance for this particular 2D gel analysis.

**Supplemental Figure 14:** Model explaining the formation of the third X-spike seen in *tlc1Δ*

*smc6-9*, *tlc1Δ smc5-31* and *tlc1Δ mms21-sp* mutants. (A) An example of a Y'-containing telomere depicting various sizes of *S. cerevisiae* telomeric Y' elements. In this example the telomere end contains a particular combination of three Y' elements, but any combination totaling between 0-4 Y'Long and Y'Short elements are possible. The sizes of the various Y' element fragments upon *Cla*I digestion are shown. (B) An aberrantly formed Rec-X intermediate is shown, that instead of linking equivalent regions of the sister chromatids, has linked the terminal Y' element to an internal Y' element within the same chromatid. (C) Digestion of the telomeric DNA with *Cla*I releases a Rec-X linked fragment of DNA containing an internal Y' element (~6.7kb) and a terminal Y' element (~5.3kb), which in this case are both derived from the same chromatid. This "H" hybrid linkage between an internal and a terminal Y'Long fragment, when run on a 2D gel, will have an X-shaped character and a size intermediate to the other Rec-X

molecules. The origin of the two “standard” X-spikes is believed to be from recombination intermediates formed between two internal Y’ elements (6.7kb + 6.7kb) [largest X-spike (spike-I)] or two terminal Y’ elements (5.3kb + 5.3kb) [smallest X-spike (spike-T)] (See Fig. 7). (D) Other potential recombination dependent linkages that could lead to the formation of the third (intermediate sized) “H” hybrid X-spike are shown. Each pair of colors represents a recombination intermediate formed between regions of homology within the same chromatid that could lead to the hybrid X-spike. We also point out that linkages do not have to be between the TG track repeats but could be between any region of the Y’ elements where homology exists; the precise point of linkage will not affect the molecular weight of the joint molecule, only where it would run along the X-spike. Finally although our models assume linkages within the same chromatid are the basis for the formation of the hybrid recombination intermediates, it is possible that a subset are formed between sister chromatids (Supplemental Figure 15) and perhaps different chromosomes. We favor an intrachromatid model because Smc5/6 encourages recombination between sister chromatids and because an intrachromatid event might be more likely than interchromosome events given relatively proximities of targets.

**Supplemental Figure 15:** An alternative to the model in Supplemental Figure 14, involving unequal sister template switch events to explain the formation of the third X-spike seen in *tlc1Δ smc6-9* and *tlc1Δ mms21-sp* mutants. (A) Diagram depicting the same Y’-containing telomere, as used in Supplemental Figure 14. (B) An aberrantly formed Rec-X intermediate is shown, that instead of linking the equivalent region of the sister chromatid, has invaded a more internal sequence. (C) Digestion of the telomeric DNA with ClaI releases a Rec-X linked fragment of DNA containing an internal Y’ element (~6.7kb) and a terminal Y’ element (~5.3kb). This “H” hybrid linkage between an internal and a terminal Y’ Long fragment when run on a 2D gel, will have an X-shaped character and a size in between other Rec-X molecules. The origin of the two “standard” X-spikes is believed to be from recombination intermediates formed between two

internal Y' elements (6.7kb + 6.7kb) [largest X-spike (spike-I)] or two terminal Y' elements (5.3kb + 5.3kb) [smallest X-spike (spike-T)]. **(D)** Other potential recombination dependent linkages that could lead to the formation of the third (intermediate sized) "H" hybrid X-spike are shown. Each pair of colors represents a recombination intermediate formed between the two sister chromatids. We also point out that linkages do not have to be between the TG track repeats but could be between any region of the Y' elements where homology between sister chromatids exists; the precise point of linkage will not affect the molecular weight of the joint molecule, only where it would run along the X-spike.

**Supplemental Figure 16:** X-structures accumulated in *smc5-6* and *smc6-9* mutants are dependent upon homologous recombination. **(A)** Representative 2D gel analysis of replication intermediates at ARS304 (similar results were obtained at ARS305) in MMS-treated cells of the indicated genotypes. **(B)** Quantification of the ratio of X-shaped molecules to structures running within the replication arc. Data represent the mean and standard error from at least two and in most cases three or more independent samples per genotype. Comparisons between *smc5-6* and *smc6-9* cells and their corresponding *rad52* double mutants were significant ( $p < 0.001$ ).

**Supplemental Figure 17:** Summary of the structure of X-shaped molecules and the various genetic and biochemical properties that each exhibit. Newly synthesized strands are shown as colored dotted lines. Parental strands are shown as solid black lines.

**Supplemental Figure 18:** Biochemical analysis of the X-shaped molecules accumulated in *mms21-sp* and *smc6-9* mutants. X-shaped molecules from *sgs1Δ* cells were used as a control since the character of X-shaped molecules within *sgs1Δ* has been previously established as being that of a Rec-X (6). **(A)** Replication intermediates from 2D gel analysis are shown and the various species of interest are labeled. **(B)** Branch migration assay showing control (non-branch



migrated),  $-Mg^{+2}$  and  $+Mg^{+2}$  (samples migrated in the absence or presence of magnesium respectively).  $Mg^{+2}$  inhibits the branch migration of HJs or regressed replication forks, while allowing for the efficient branch migration of Rec-X intermediates. Branch migration was performed in gel slices from the first dimension and prior to running the second dimension. (C) Quantification of the ratio of X-shaped molecules to the migrated X-spike for the data shown in panel B. No difference in branch migration in the absence or presence of magnesium was observed. An ARS304 probe was used.

**Supplemental Figure 19:** Biochemical analysis of the X-shaped molecules accumulated in *mms21-sp* and *smc6-9* mutants. X-shaped molecules from *sgs1Δ* cells were used as a control since the character of X-shaped molecules within *sgs1Δ* has been previously established as being that of a Rec-X (6). (A) Replication intermediates of interest are highlighted. (B) Diagram showing the processing of Rec-X intermediates by Mung Bean nuclease. Mung Bean nuclease has activity against single stranded DNA regions and would be expected to convert Rec-X recombination intermediates into DNA structures that have a migration pattern similar to that of convergent replication forks, when samples are digested with Mung Bean before running in the first dimension. (C) Results of Mung Bean assay, showing X-shaped molecules being converted into structures with a migration pattern similar to that of convergent replication forks. The lack of complete conversion is attributed to an insufficient amount of time during Mung Bean digestion. This is supported by the lack of complete digestion within the X-spike of *sgs1Δ* cells which have previously been shown to accumulate mostly Rec-X recombination intermediates within their X-spike (6). An ARS304 probe was used.

**Supplemental Figure 20:** Model depicting a template switch recombination repair pathway. The physical linkage seen before the initiation of template switch recombination depicts that of a hemicatenane that is thought to travel behind the fork and assist in template switching. At a stall-

inducing lesion (*circle*) the sister is used as a template to allow lesion bypass. Rad52-dependent HR enables reinvasion of the original template, and after completion of replication sumoylation and Smc5/6 work with Sgs1 to resolve the Rec-X intermediate. The figure is based on Liberi et al., 2005 and Lee et al, 2007 (6,7).

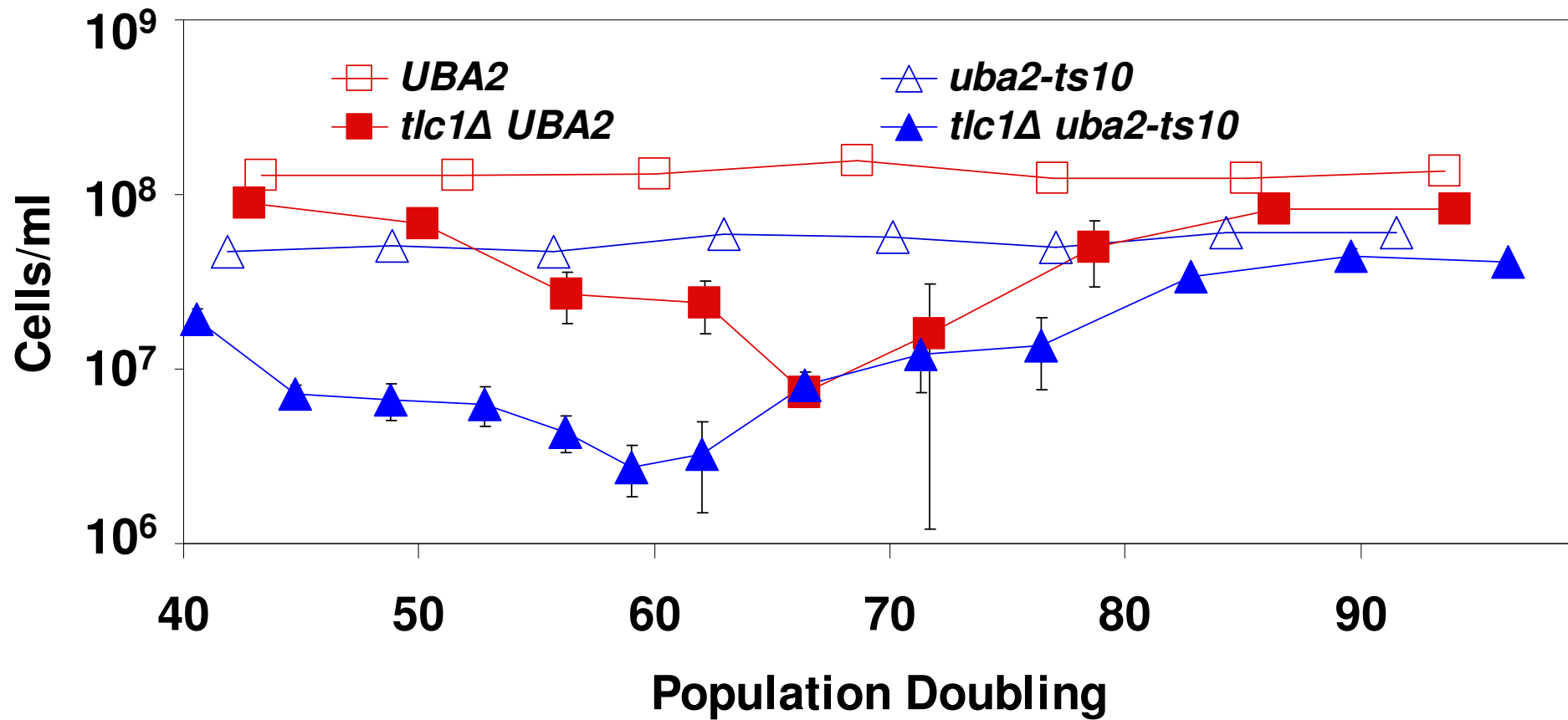
**Supplemental Figure 21:** Biochemical analysis of the X-shaped molecules accumulated at the telomere in *tlc1Δ smc6-9* mutants. Branch migration assay showing control (non-branch migrated), -Mg<sup>+2</sup> and +Mg<sup>+2</sup> (samples migrated in the absence or presence of magnesium respectively). Mg<sup>+2</sup> inhibits the branch migration of HJs and regressed replication forks, while allowing for the efficient branch migration of Rec-X intermediates. No difference in branch migration in the absence or presence of magnesium was observed. Although the appearance of two novel spikes is observed in samples migrated in the presence +Mg<sup>+2</sup>, these spikes are clearly distinct from the X-spikes and most likely represent the stabilization of reversed replication forks by Mg<sup>+2</sup>. Their appearance at branch migrated telomere replication forks but not at other tested genomic loci is likely due to the promotion of spontaneous fork reversal by repetitive TG track sequences (8). The Y'-Long telomere probe was used.

#### Supplemental References

1. Ghaemmaghami, S., Huh, W. K., Bower, K., Howson, R. W., Belle, A., Dephoure, N., O'Shea, E. K., and Weissman, J. S. (2003) *Nature* **425**, 737-741
2. Panse, V. G., Hardeland, U., Werner, T., Kuster, B., and Hurt, E. (2004) *J Biol Chem* **279**, 41346-41351
3. Nugent, C. I., Bosco, G., Ross, L. O., Evans, S. K., Salinger, A. P., Moore, J. K., Haber, J. E., and Lundblad, V. (1998) *Current Biology* **8**, 657-660
4. Polotnianka, R. M., Li, J., and Lustig, A. J. (1998) *Curr Biol* **8**, 831-834.
5. Cost, G. J., and Cozzarelli, N. R. (2006) *Genetics* **172**, 2185-2200
6. Liberi, G., Maffioletti, G., Lucca, C., Chiolo, I., Baryshnikova, A., Cotta-Ramusino, C., Lopes, M., Pelliccioli, A., Haber, J. E., and Foiani, M. (2005) *Genes Dev* **19**, 339-350
7. Lee, J., Kozak, M., Martin, J., Pennock, E., and Johnson, F. B. (2007) *PLOS Biology* **5**, e160

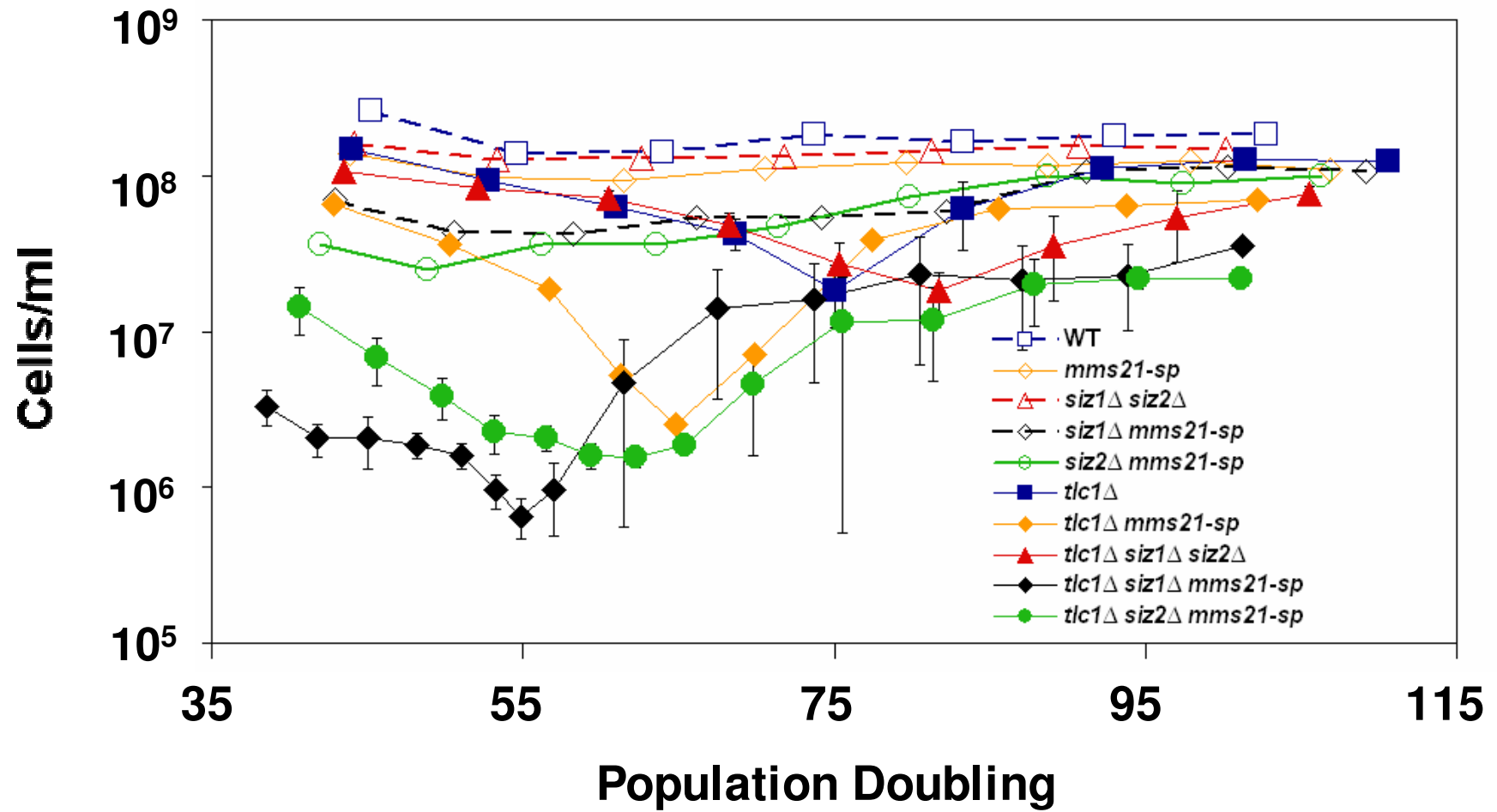
8. *Fouche, N., Ozgur, S., Roy, D., and Griffith, J. D. (2006) Nucleic Acids Res 34, 6044-6050*

# Supplemental Figure 1

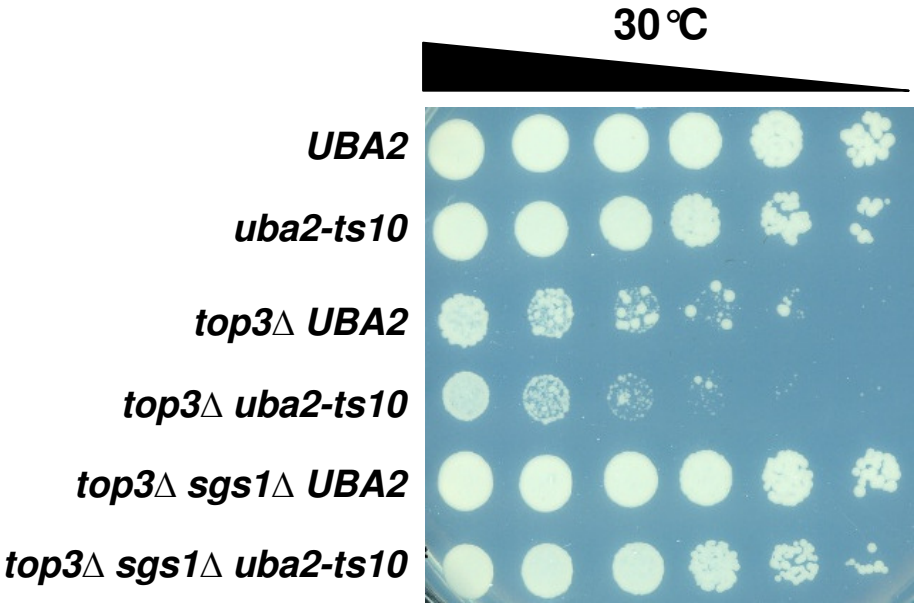




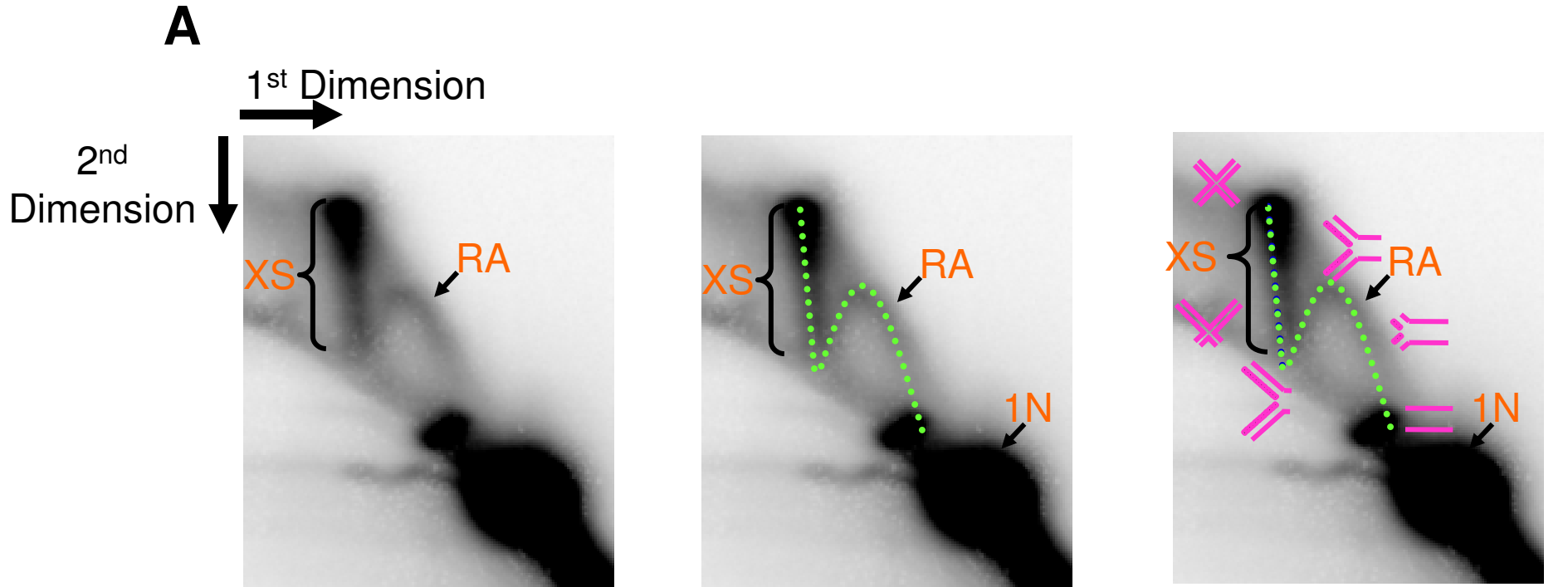
# Supplemental Figure 3



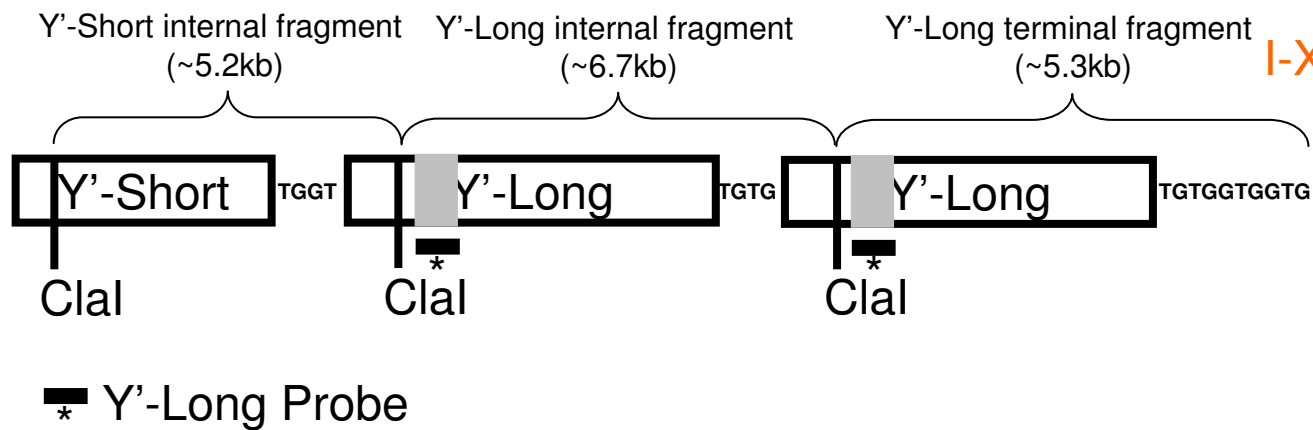
# Supplemental Figure 4



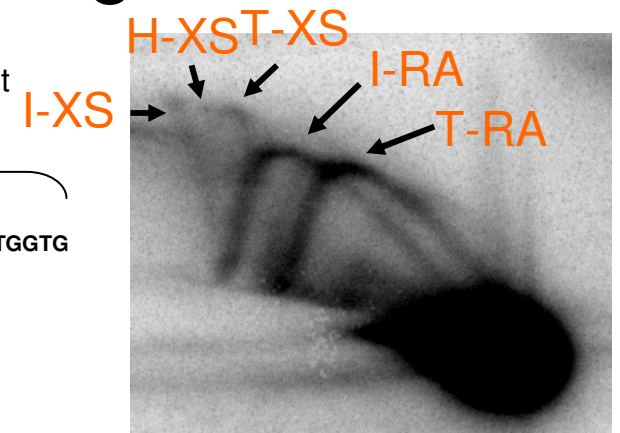
# Supplemental Figure 5A-B



**B**



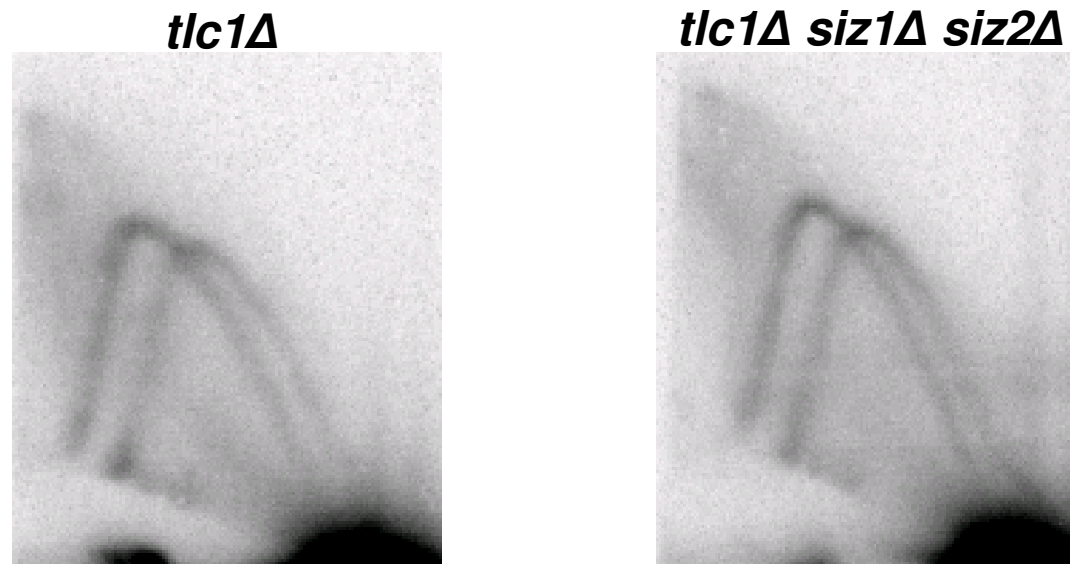
**C**



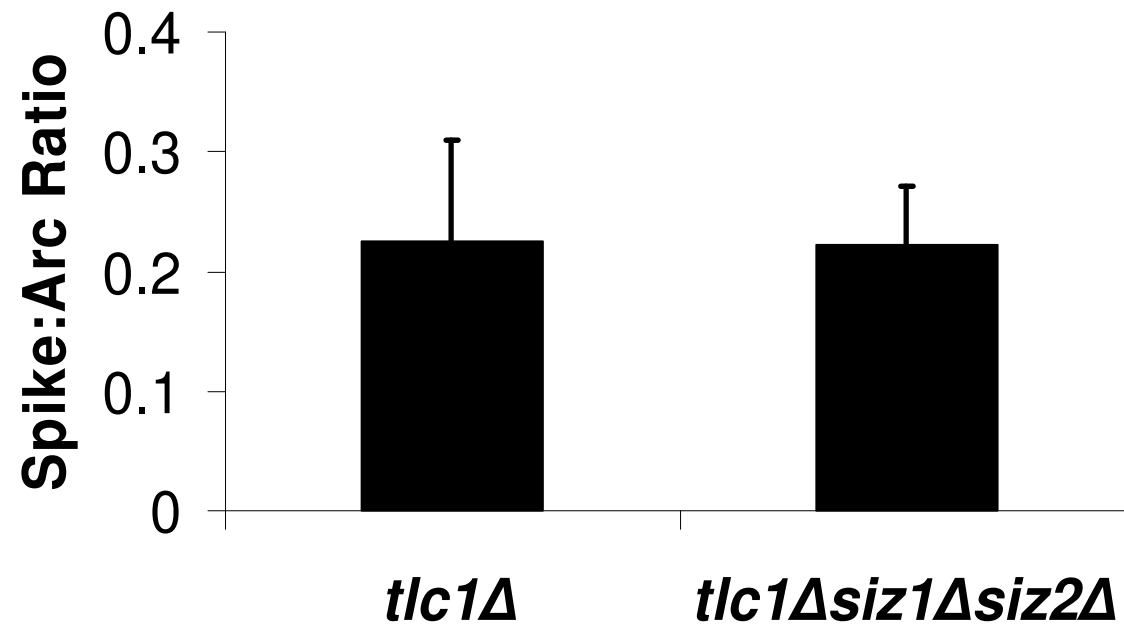


# Supplemental Figure 6A-B

**A**

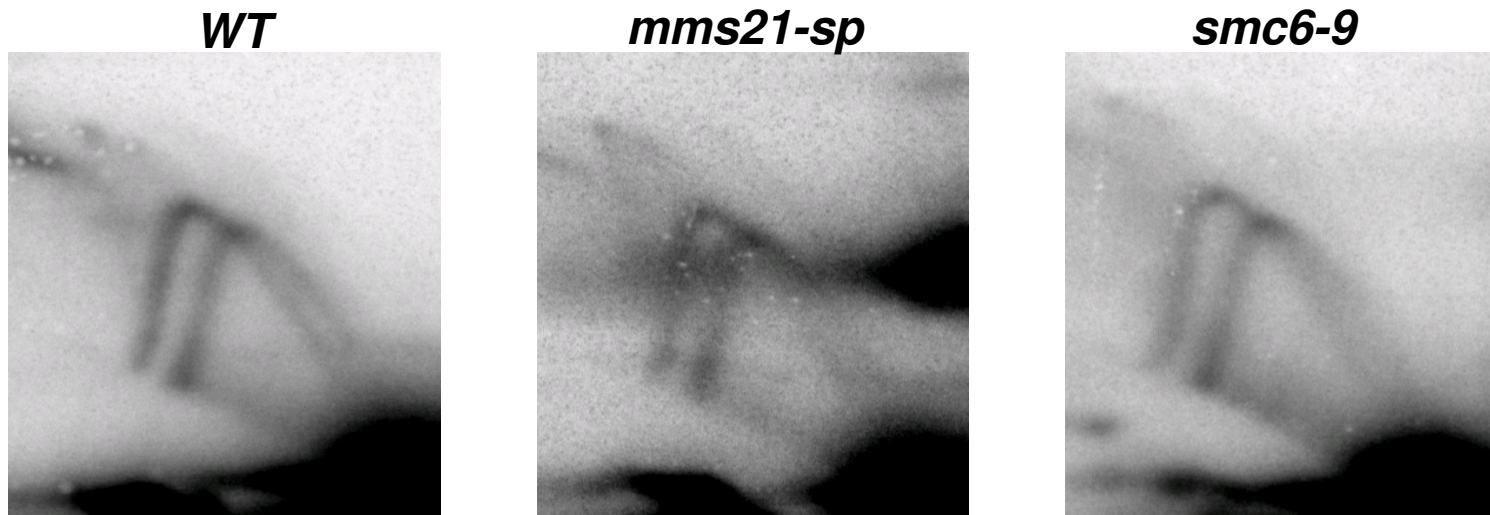


**B**

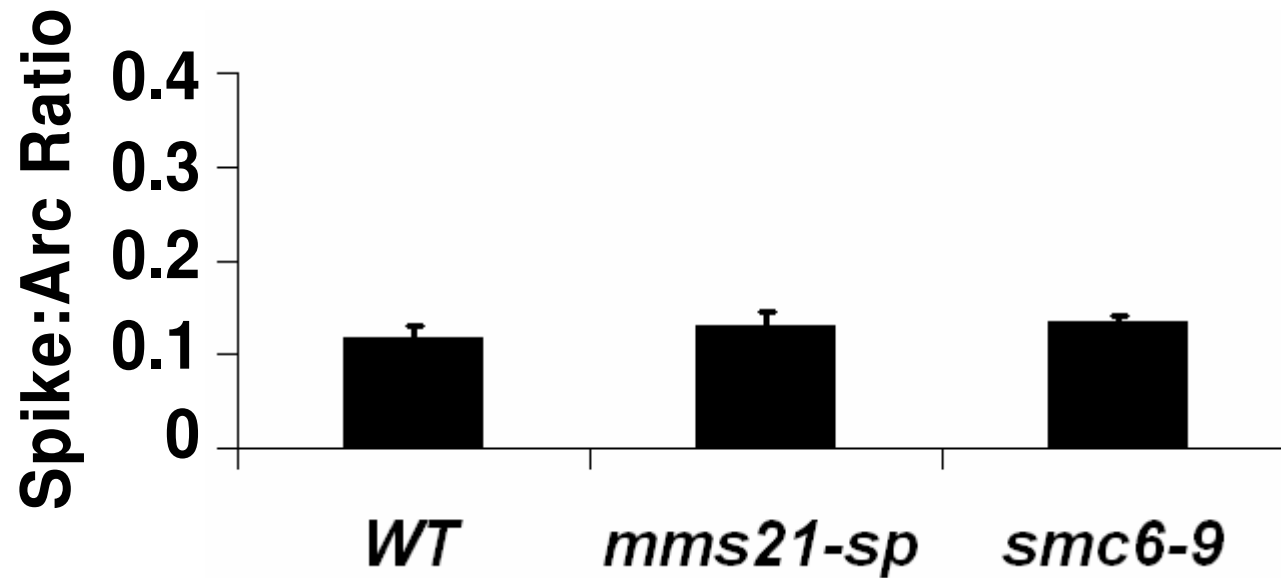


# Supplemental Figure 7A-B

**A**

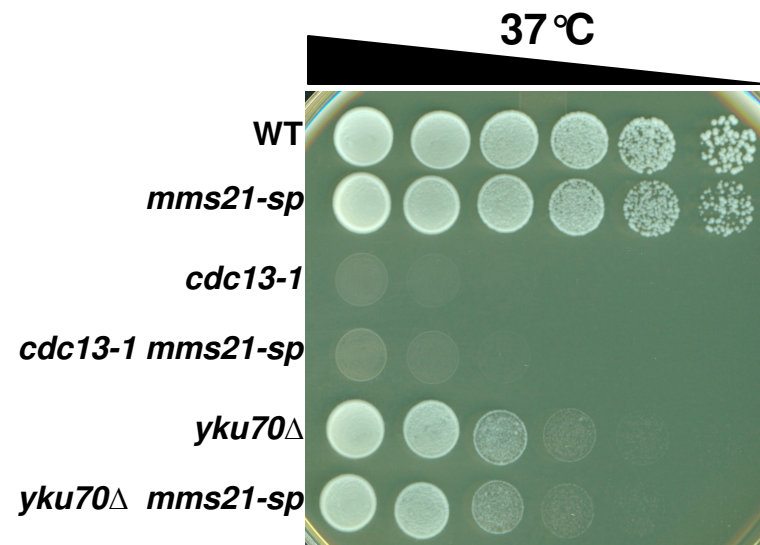
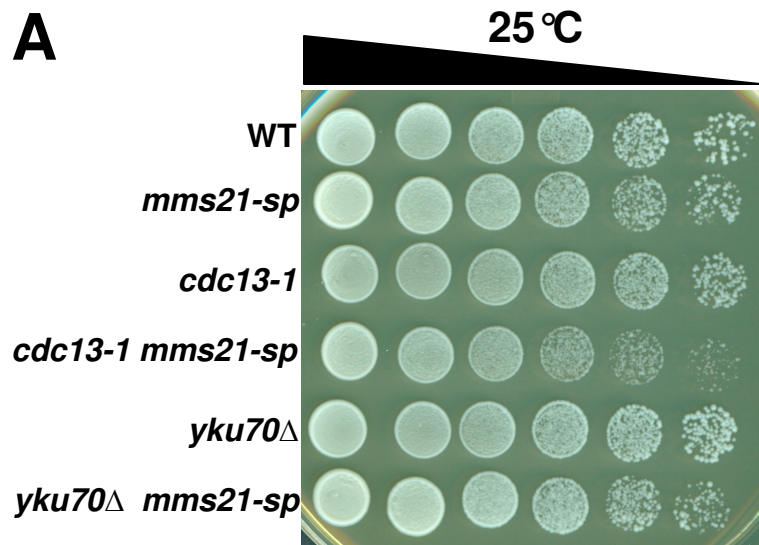


**B**

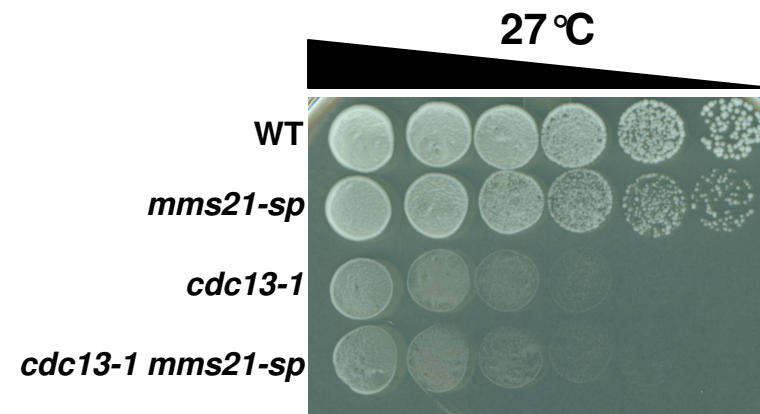
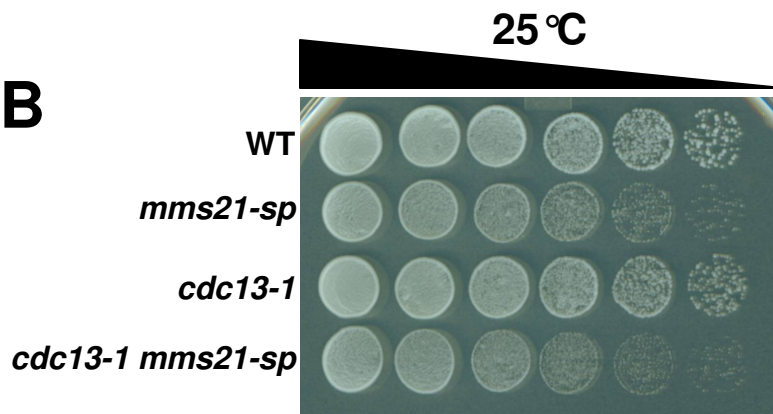


# Supplemental Figure 8A-B

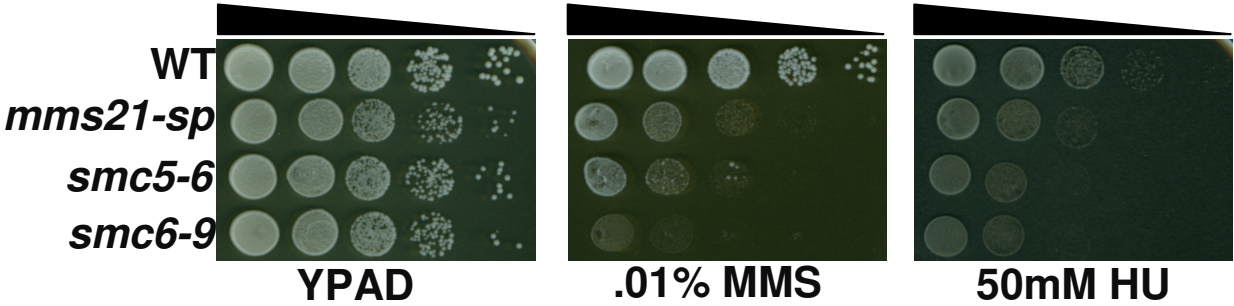
## A



## B

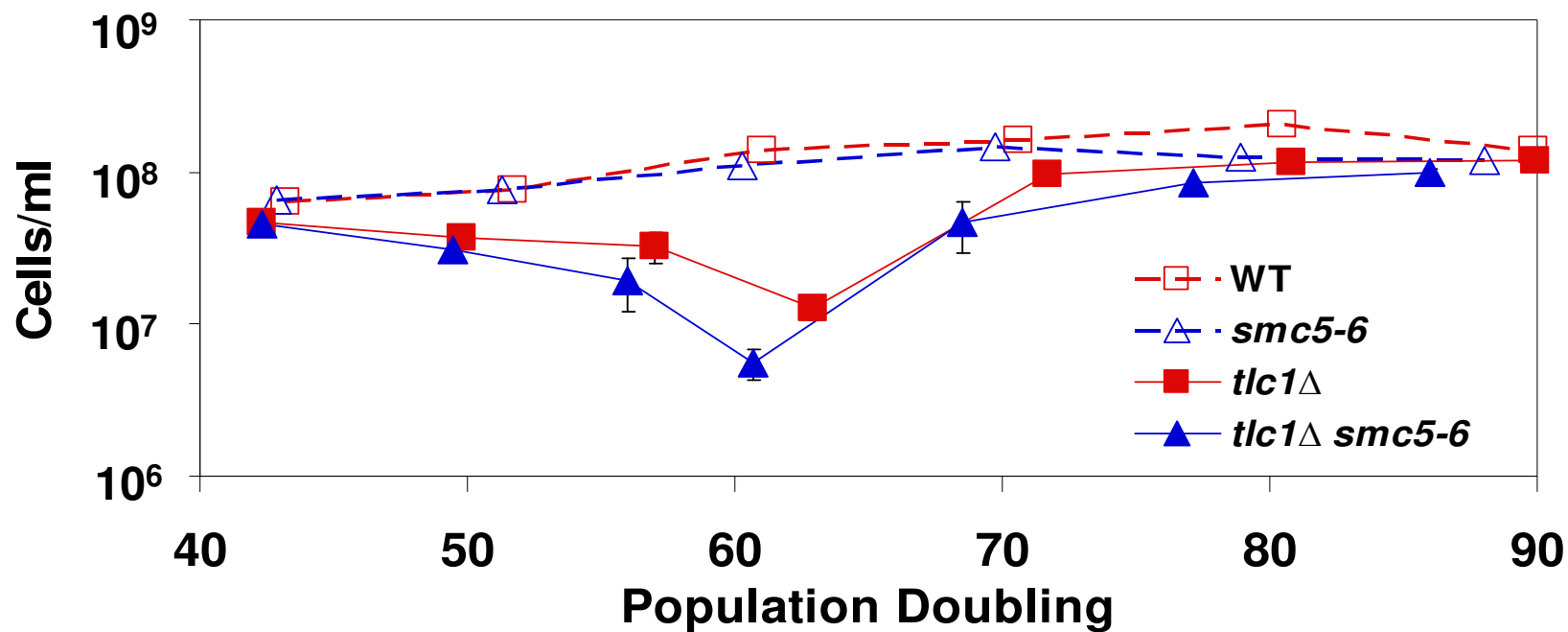


# Supplemental Figure 9

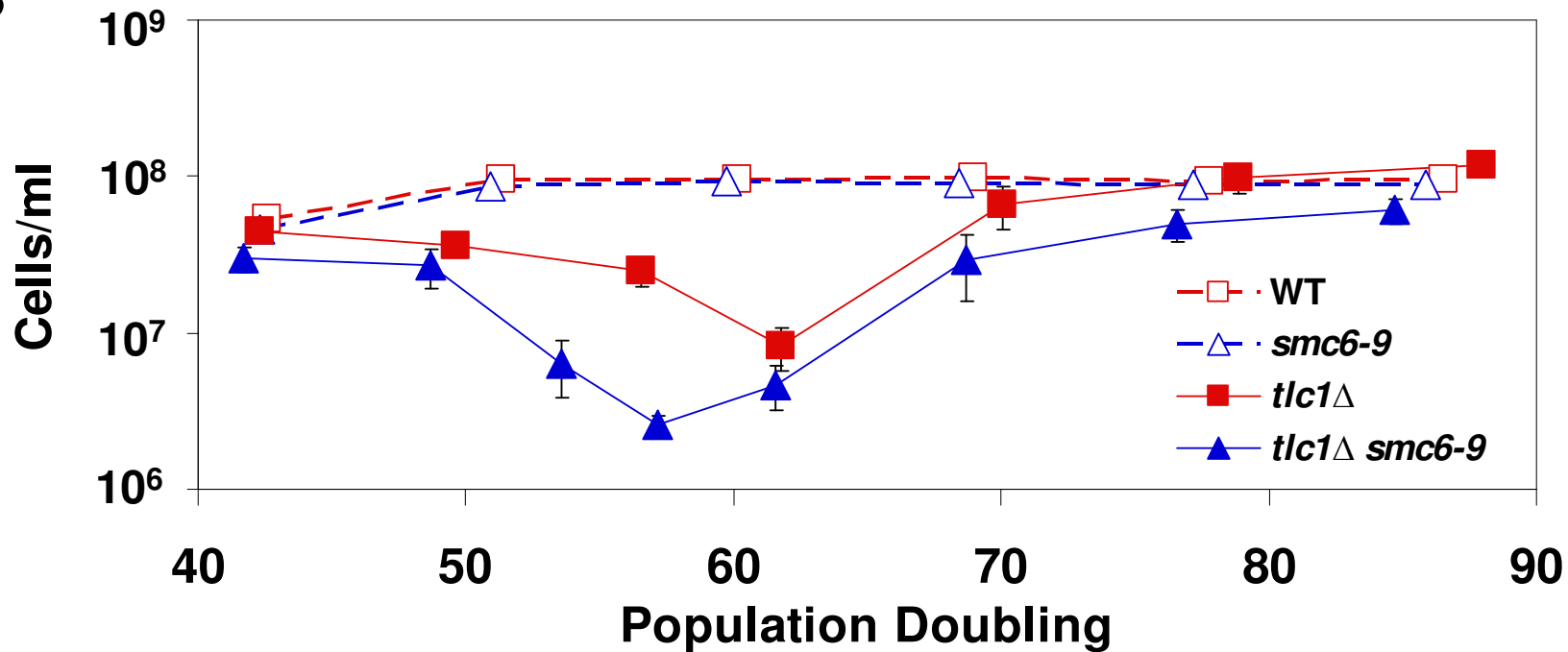


# Supplemental Figure 10

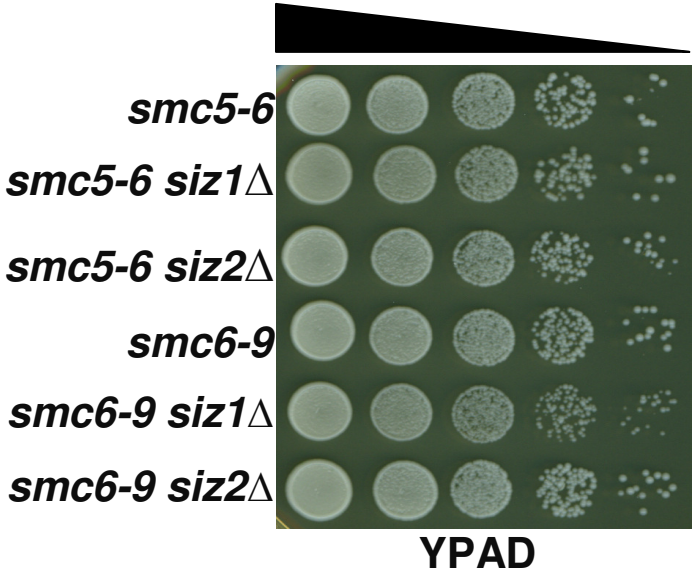
## A



## B



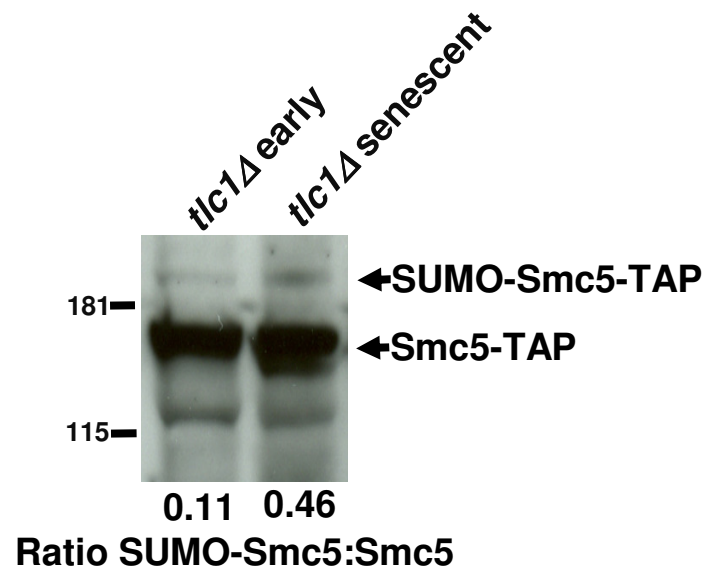
# Supplemental Figure 11



# Supplemental Figure 12A-B

## A

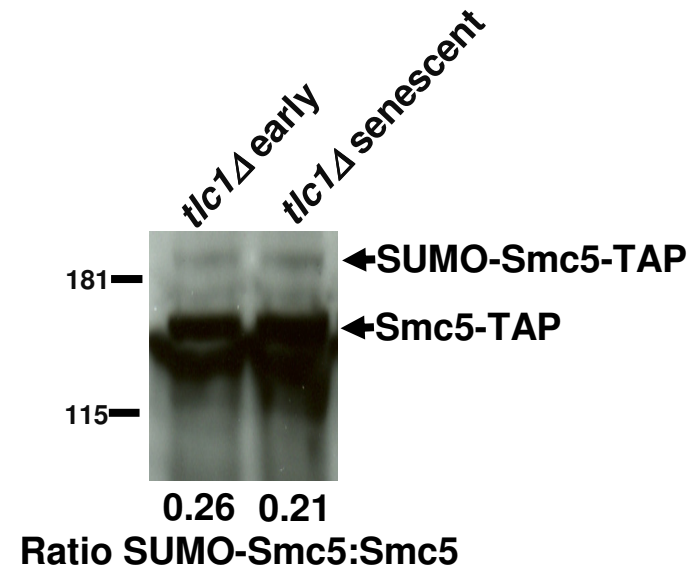
*tlc1* $\Delta$  *smc5-TAP*



Underexposed Smc5-TAP band used for quantification

## B

*tlc1* $\Delta$  *mms21-sp*  
*smc5-TAP*

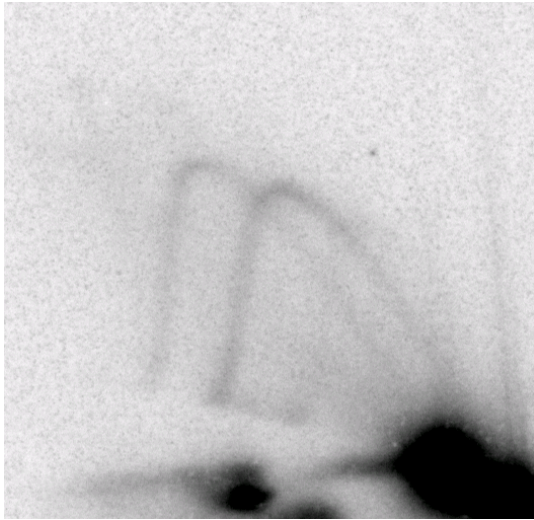


Underexposed Smc5-TAP band used for quantification

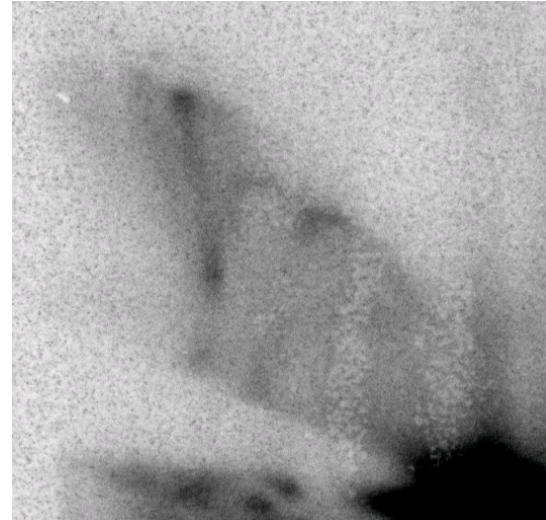
# Supplemental Figure 13A-B

**A**

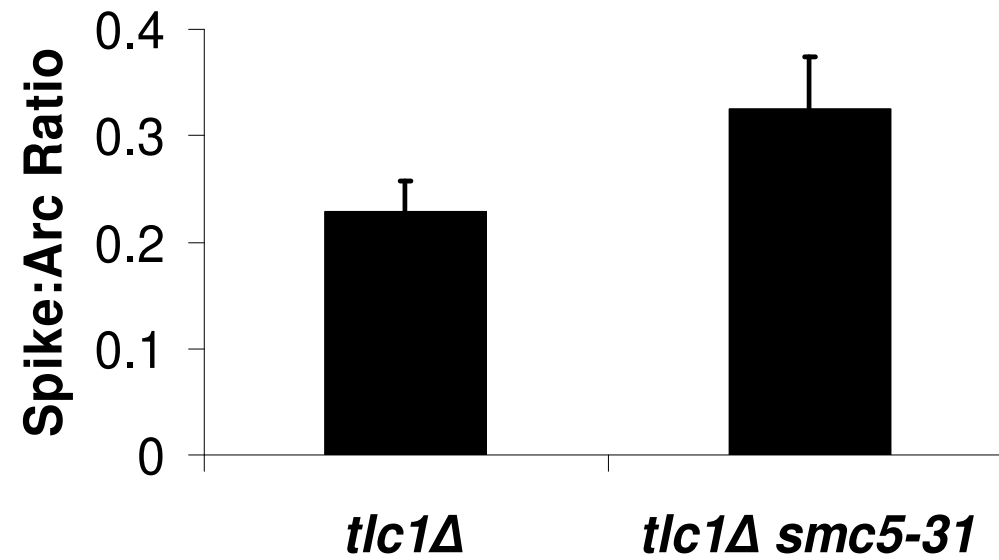
*tlc1Δ*



*tlc1Δ smc5-31*

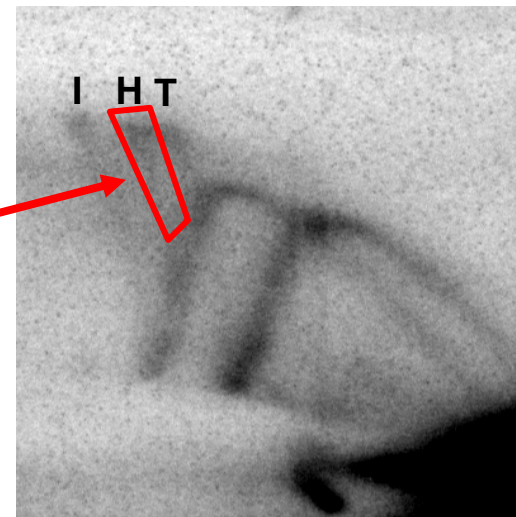
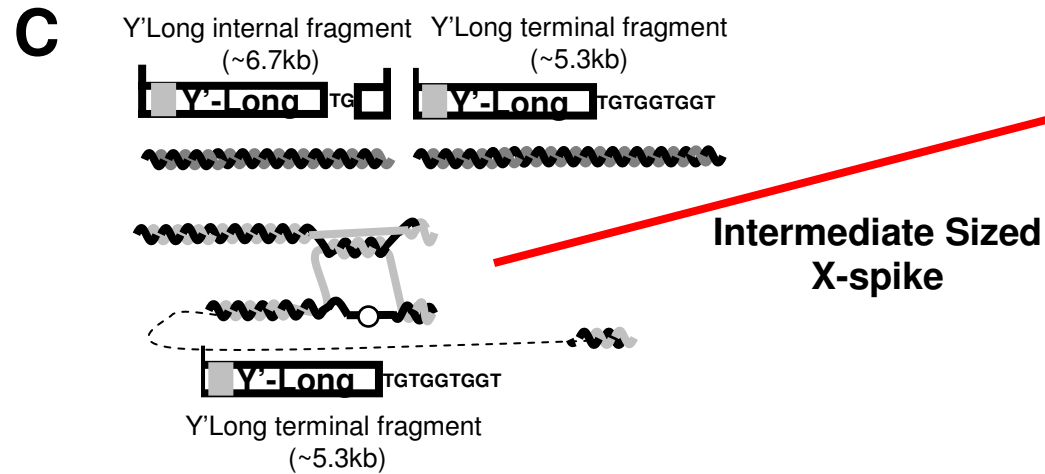
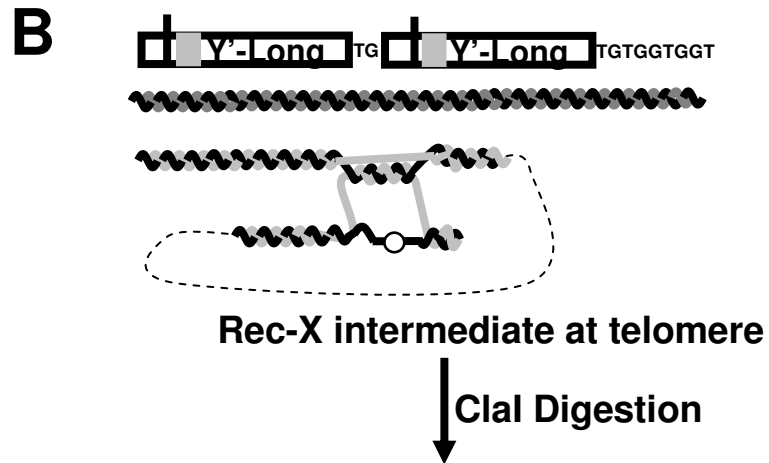
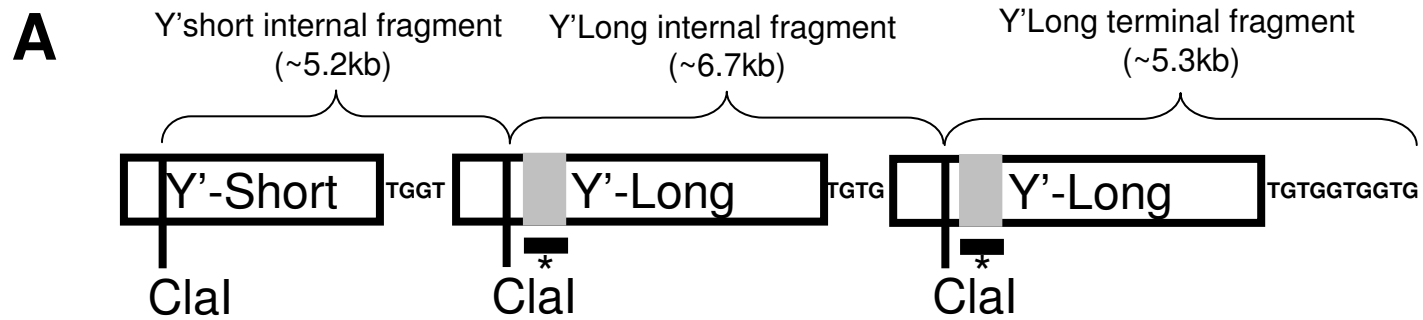


**B**



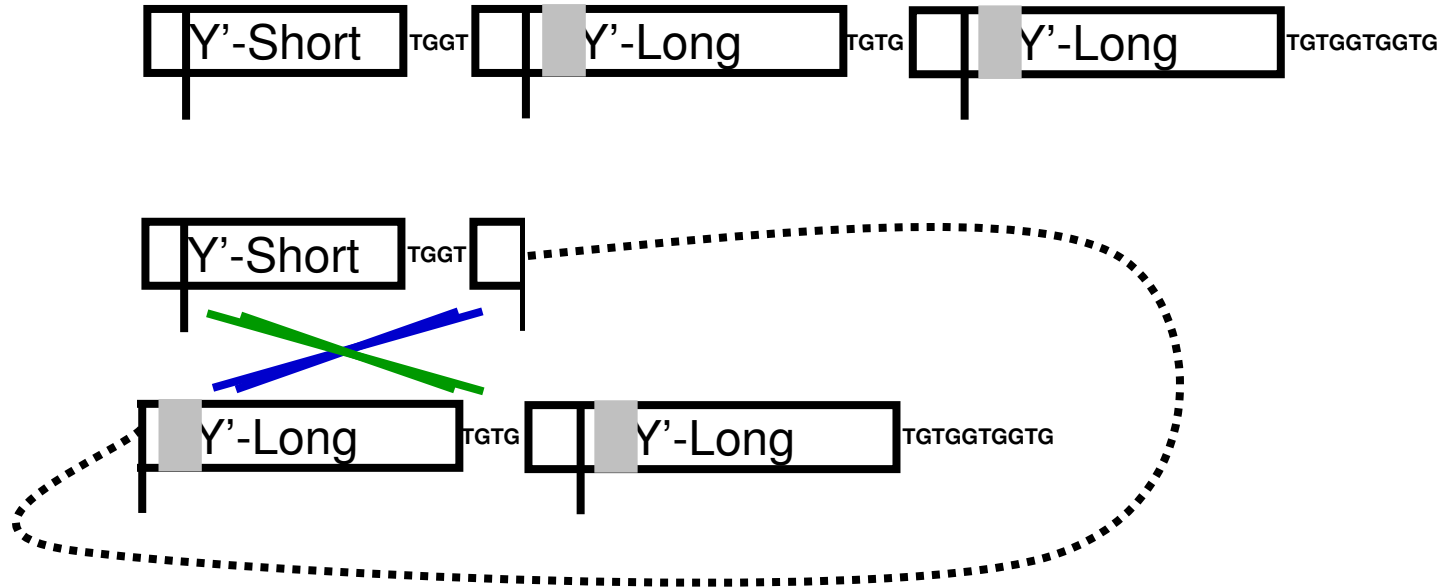


# Supplemental Figure 14A-C

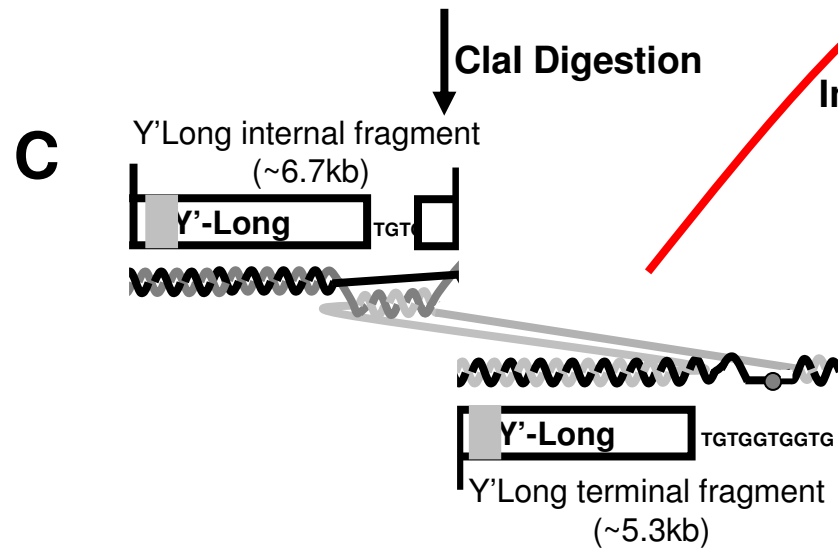
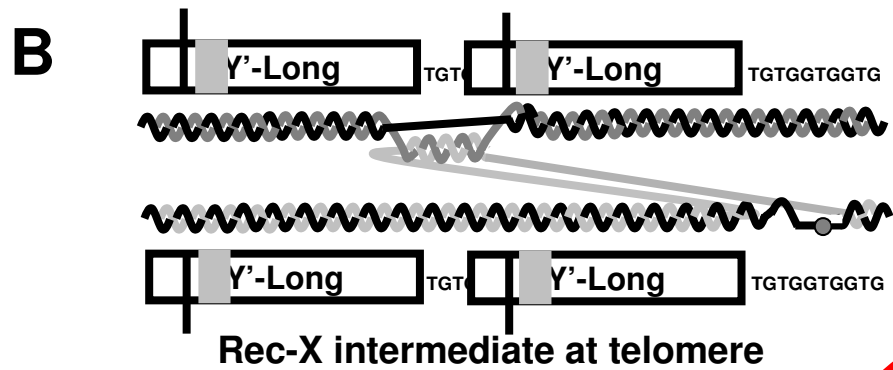
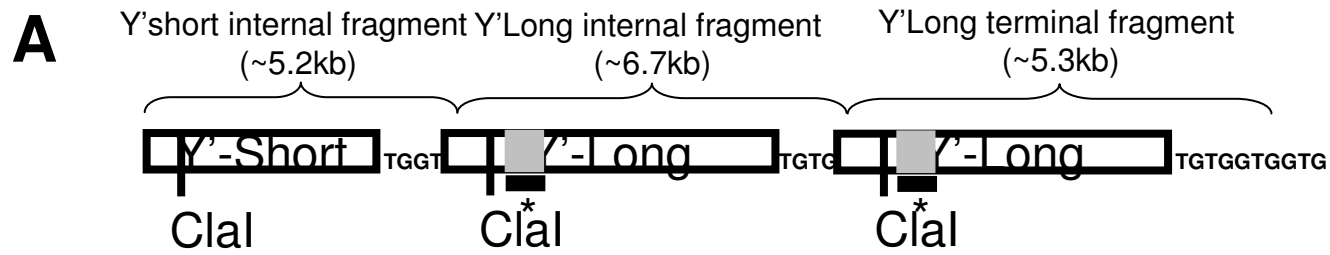


# Supplemental Figure 14D

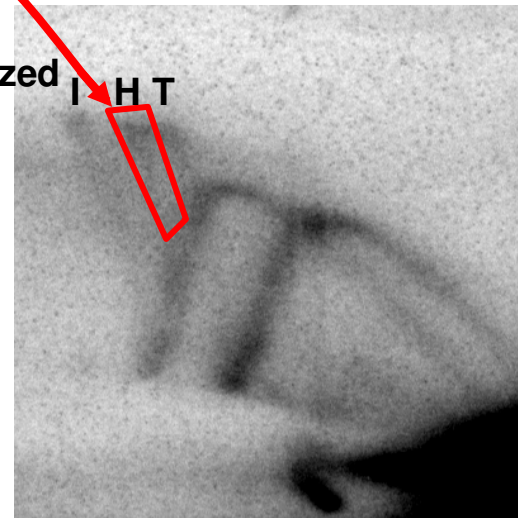
**D**



# Supplemental Figure 15A-C

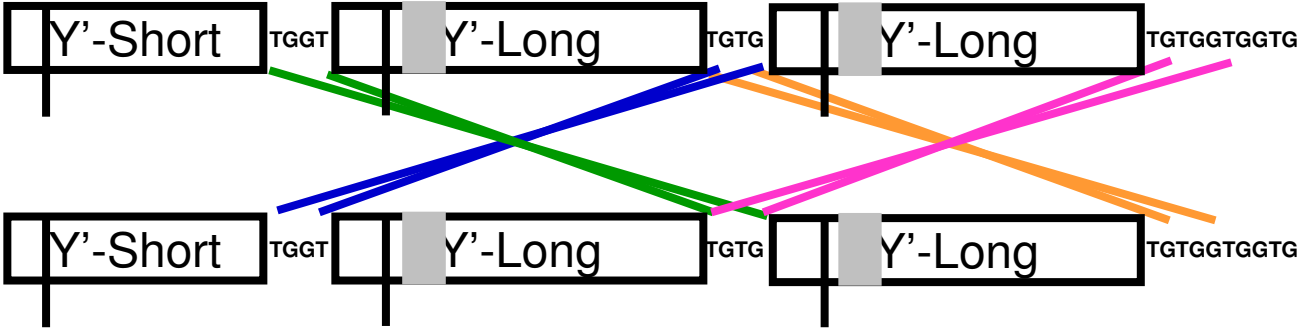


Intermediate Sized X-spike



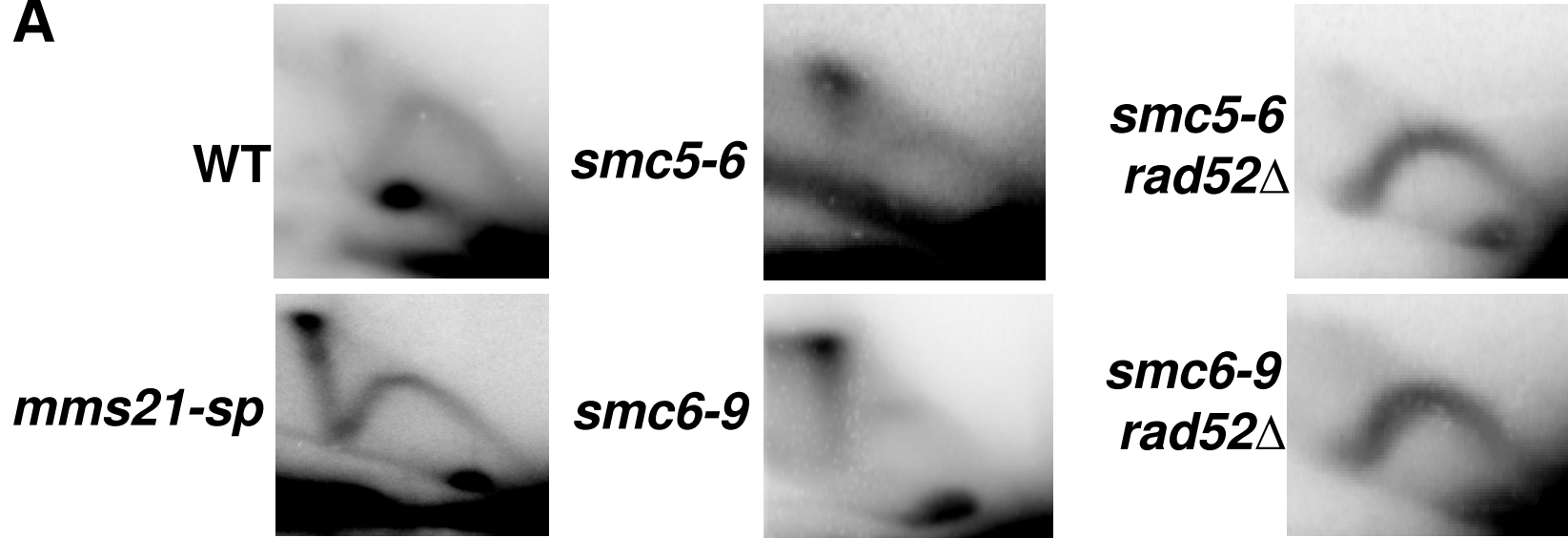
# Supplemental Figure 15D

D

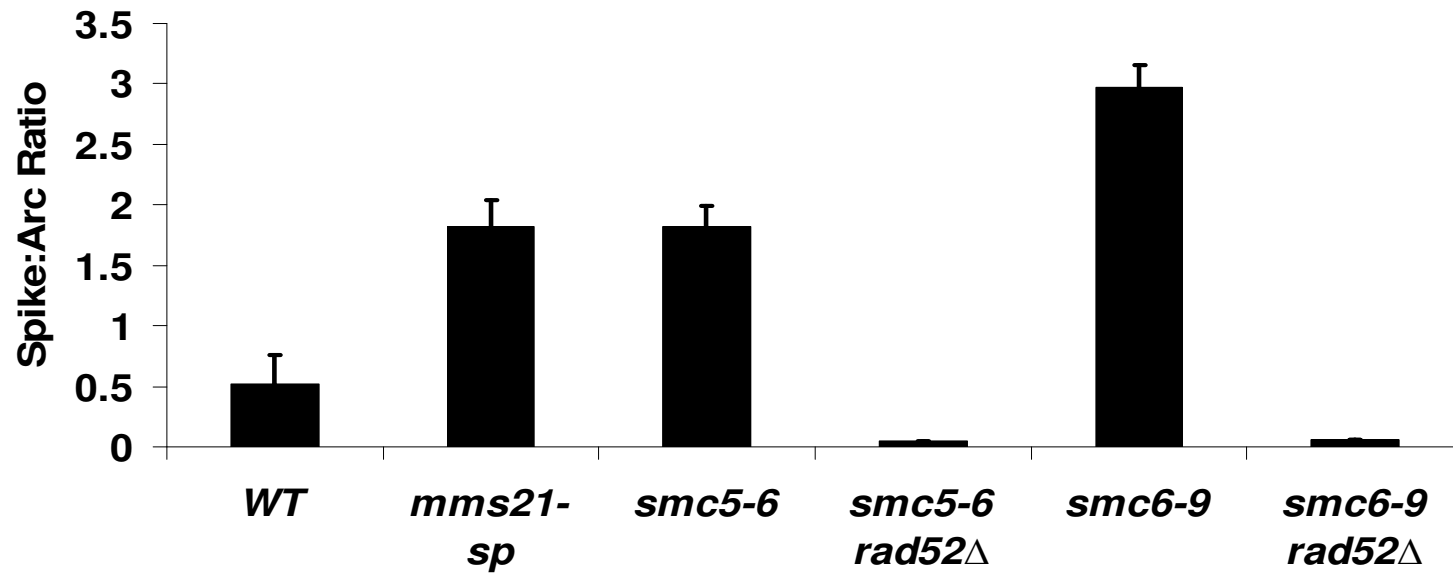


# Supplemental Figure 16A-B

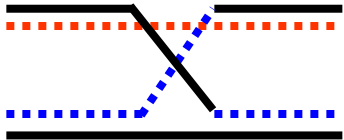
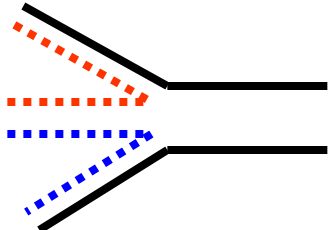
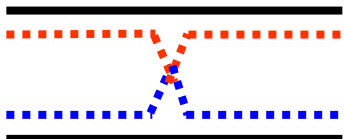
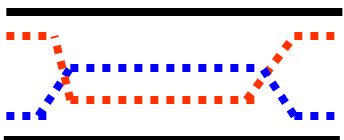
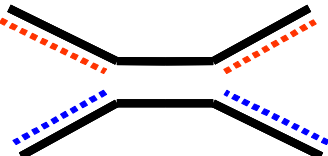
**A**



**B**

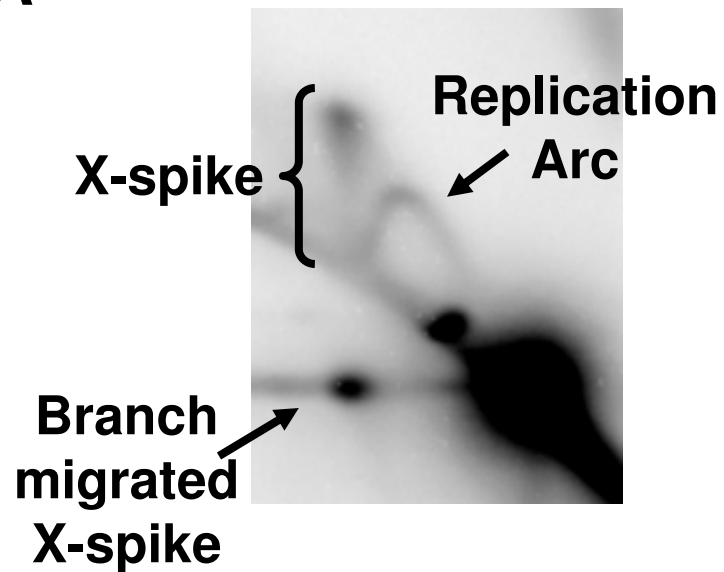


# Supplemental Figure 17

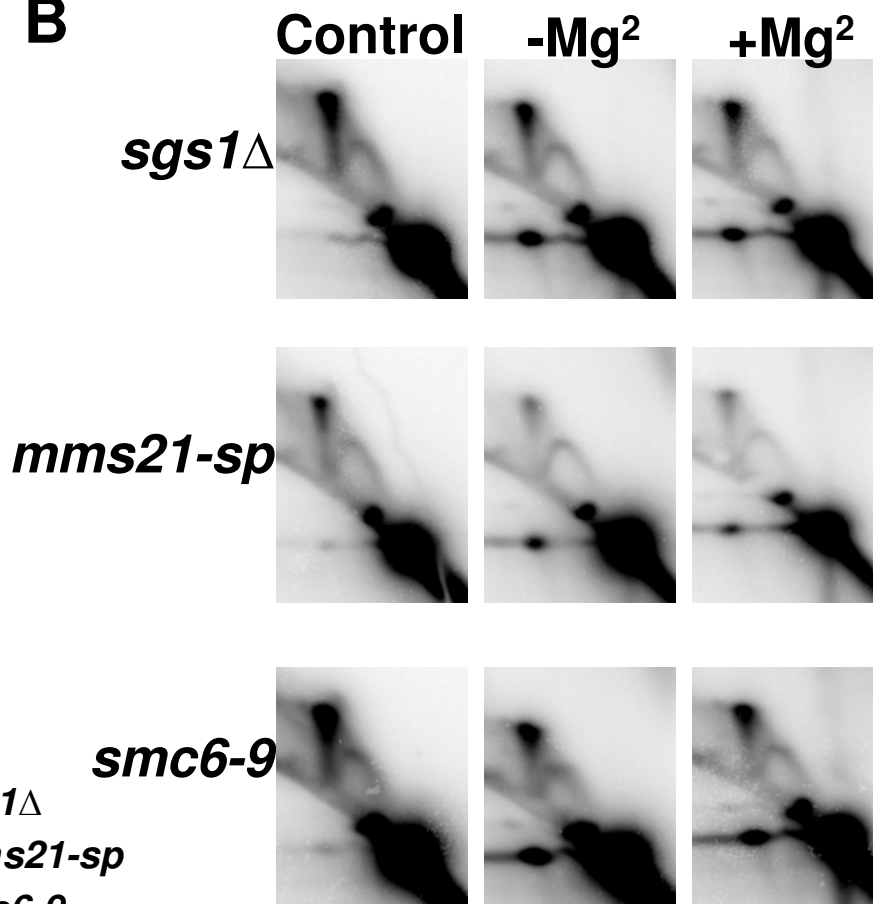
|   | Rad52<br>Dependent | Branch<br>Migratable | Branch<br>Migratable<br>In Presence<br>of Mg <sup>++</sup> | Mung Bean<br>Nuclease<br>Sensitive |
|---|--------------------|----------------------|--|------------------------------------|
|  <b>Holliday<br/>Junction</b>                  | +                  | +                    | -  | -                                  |
|  <b>Regressed<br/>Fork</b>                     | -                  | +                    | -  | -                                  |
|  <b>Hemicatenane</b>                           | -                  | +                    | +  | -                                  |
|  <b>Rec-X</b>                                | +                  | +                    | +  | +                                  |
|  <b>Convergent<br/>Replication<br/>Forks</b> | -                  | -                    | -  | -                                  |

# Supplemental Figure 18A-C

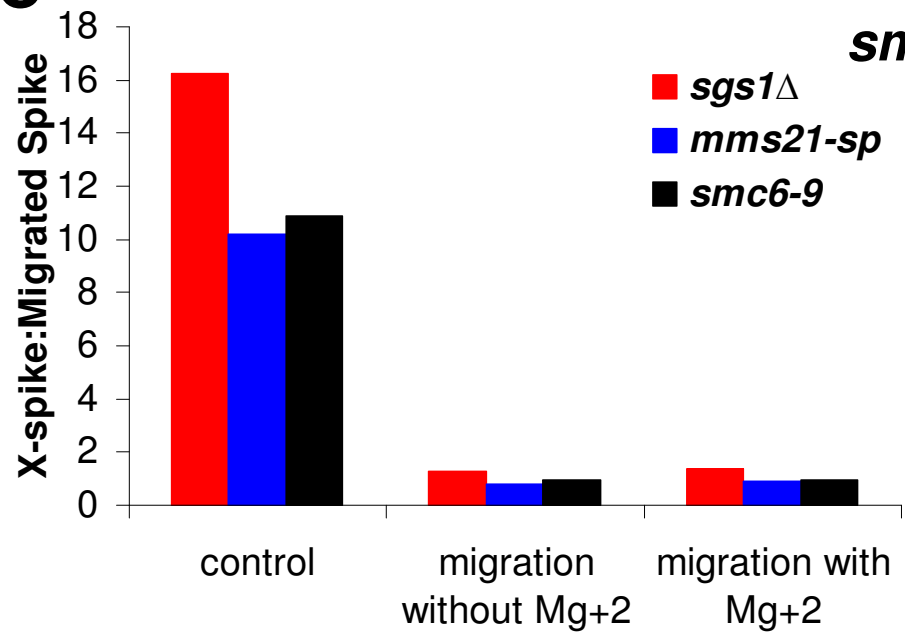
**A**



**B**

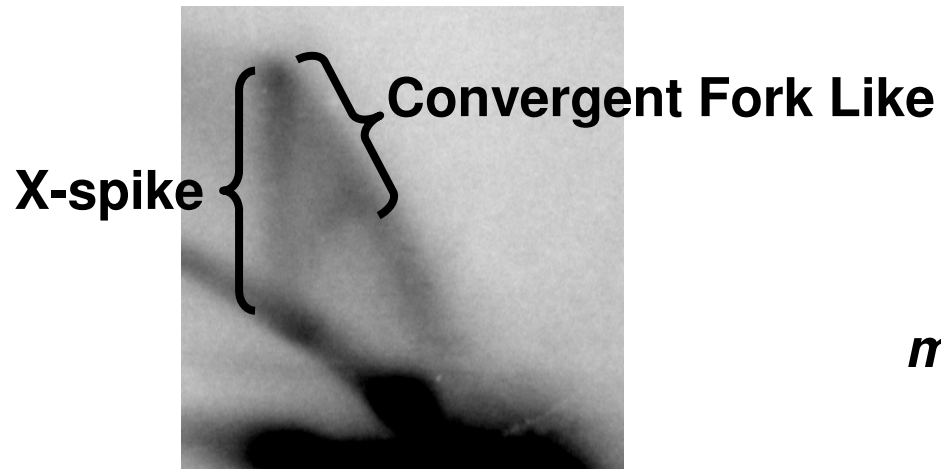


**C**

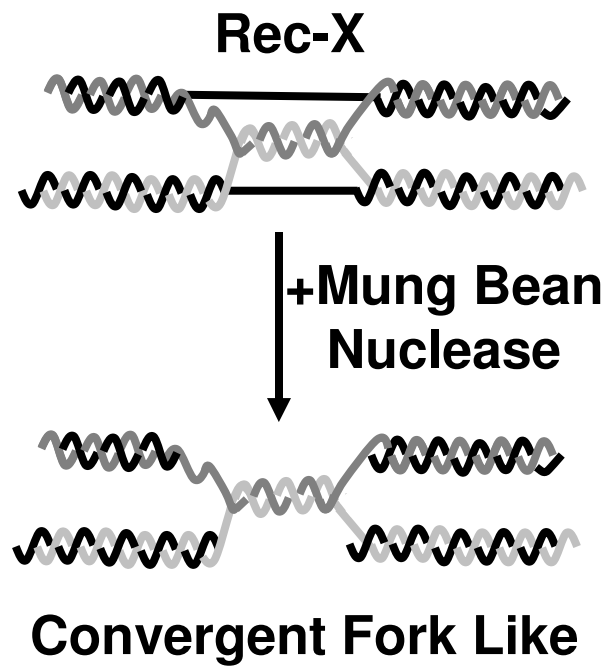


# Supplemental Figure 19A-C

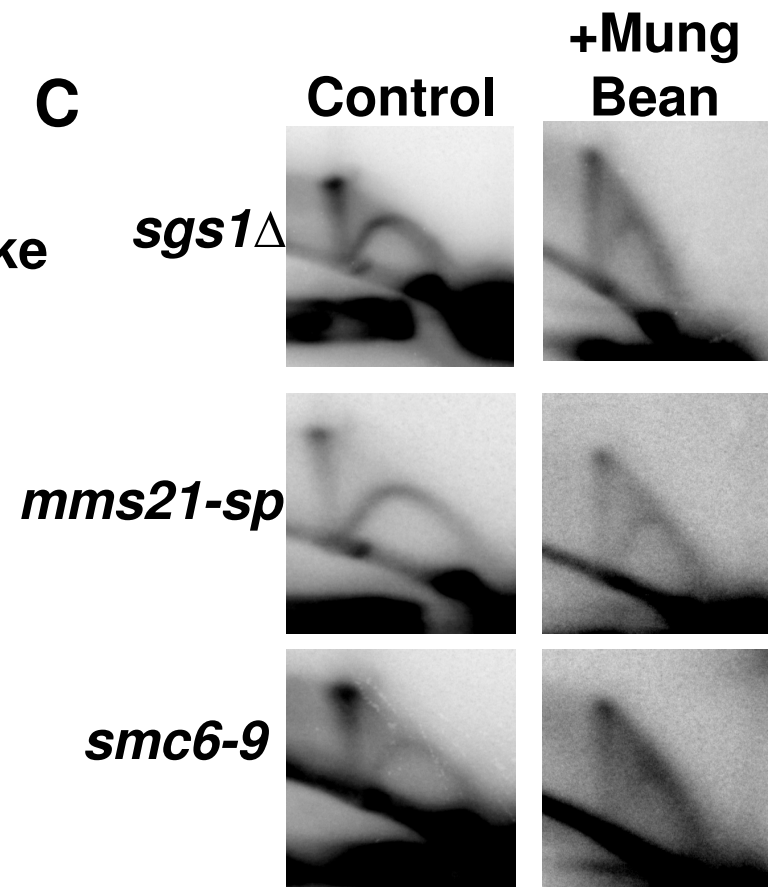
**A**



**B**

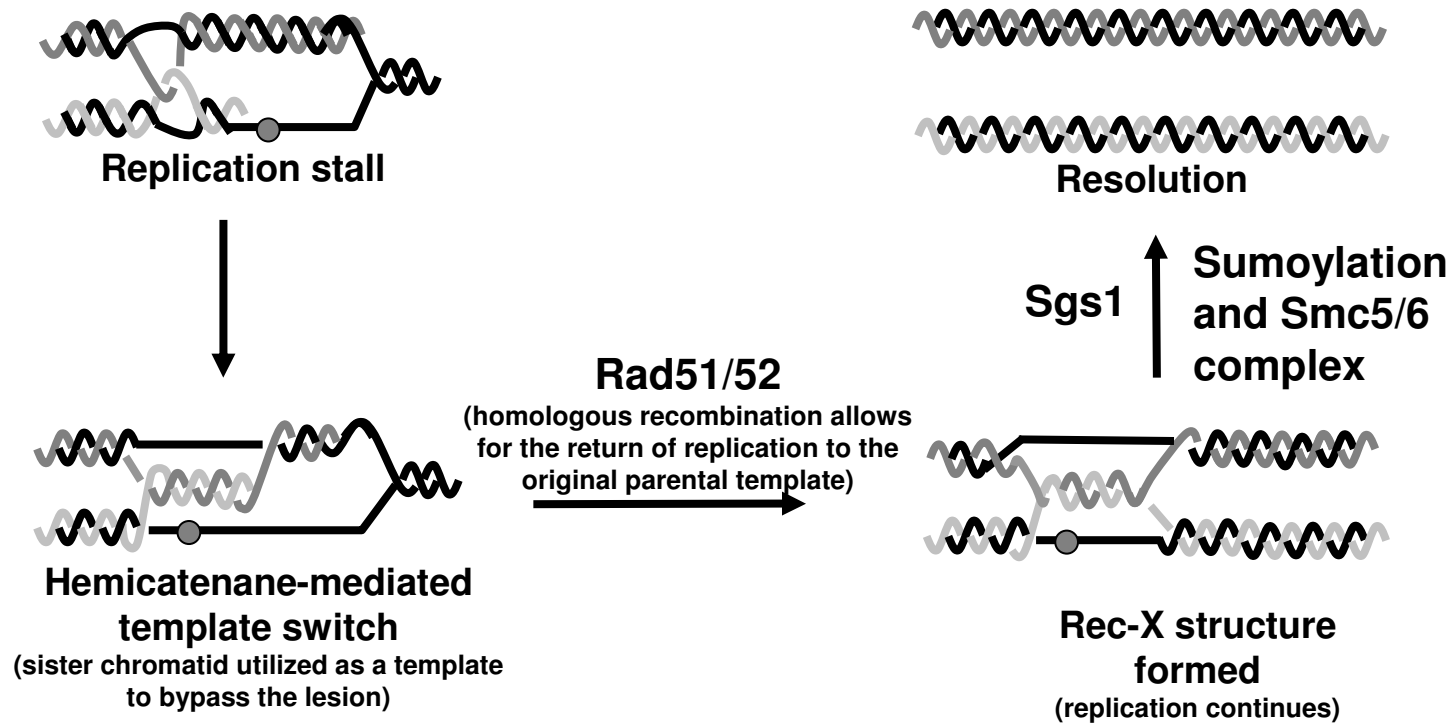


**C**

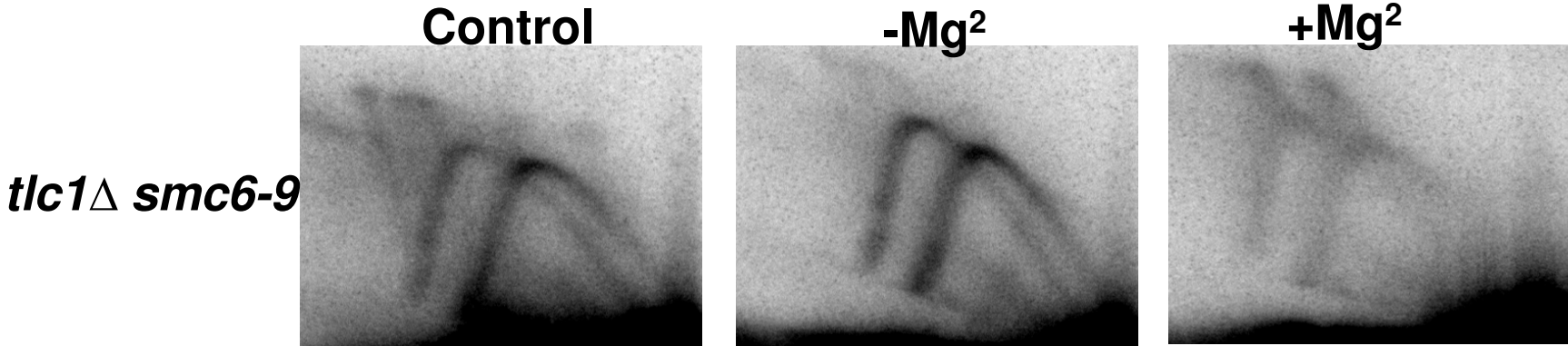




# Supplemental Figure 20



Supplemental Figure 21



# Supplemental Table 1

List of candidate genes screened for sumoylation in the absence or presence of MMS

|       |       |       |       |
|-------|-------|-------|-------|
| Mre11 | Rad50 | Xrs2  | Rad51 |
| Rad54 | Rad55 | Rad57 | Rad59 |
| Rmi1  | Top3  | Clb2  | Rfa1  |
| Rfa2  | Rfa3  | Kre29 | Nse6  |
| Rad53 |       |       |       |

## Supplemental Table 2

Sumoylation of several recombination factors is not dependent upon Mms21 activity

| <b>Protein</b> | <b>MMS stimulated<sup>a</sup></b> | <b>E3 ligase<sup>b</sup></b> | <b>Sumo #<sup>c</sup></b> |
|----------------|-----------------------------------|------------------------------|---------------------------|
| Rad59          | +                                 | Siz2                         | ≥2                        |
| Rfa1           | +                                 | Siz2                         | ≥2                        |
| Rfa2           | +                                 | Siz1/2                       | ≥1                        |
| Rfa3           | +                                 | Siz2                         | ≥2                        |

<sup>a</sup>sumoylation was stimulated by MMS <sup>b</sup>E3 ligase responsible for the majority of the MMS stimulated sumoylation <sup>c</sup>indicates the number of SUMO molecules predicted to be attached to the protein

### Supplemental Table 3:

|                    |  |
|--------------------|--|
| YBJ426             | MATa/ $\alpha$ , <i>his3<math>\Delta</math>/his3<math>\Delta</math>, leu2<math>\Delta</math>/leu2<math>\Delta</math>, ura3<math>\Delta</math>/ura3<math>\Delta</math>, MET15/met15<math>\Delta</math>, LYS2/<math>\Delta</math>lys2, TLC1/<math>\Delta</math>tlc1::LEU2, cir<sup>+</sup></i> |
| YAC18              | YBJ426 <i>UBA2/uba2<math>\Delta</math>::HygB</i>   |
| YAC24              | YAC18 <i>cir<sup>0</sup></i>   |
| YAC25              | YAC24 <i>pRS316-UBA2</i>   |
| YAC26              | YAC24 <i>pRS316-uba2-ts10</i>  |
| CGC1428*           | MATa, <i>bar1<math>\Delta</math> leu2-3,112 ura3-52 his3-<math>\Delta</math>200 trp1-<math>\Delta</math>63 ade2-1 lys2-801 pep4, smc6-9-3HA::HIS3</i>  |
| CGC1429*           | MATa, <i>bar1<math>\Delta</math> leu2-3,112 ura3-52 his3-<math>\Delta</math>200 trp1-<math>\Delta</math>63 ade2-1 lys2-801 pep4, smc5-6-3HA::HIS3</i>  |
| YAC166             | MATa/ $\alpha$ , <i>TOP3/top3<math>\Delta</math>::KanMX, UBA2/uba2<math>\Delta</math>::HygB, SGS1/sgs1<math>\Delta</math>::HIS3, pRS316-UBA2, cir<sup>0</sup></i>  |
| YAC168             | MATa/ $\alpha$ , <i>TOP3/top3<math>\Delta</math>::KanMX, UBA2/uba2<math>\Delta</math>::HygB, SGS1/sgs1<math>\Delta</math>::HIS3, pRS316-uba2-ts10, cir<sup>0</sup></i>   |
| YAC169             | MATa/ $\alpha$ , <i>UBA2/uba2<math>\Delta</math>::HygB, pRS316-UBA2, cir<sup>0</sup></i>   |
| YAC171             | MATa/ $\alpha$ , <i>UBA2/uba2<math>\Delta</math>::HygB, pRS316-uba2-ts10, cir<sup>0</sup></i>  |
| YAC184             | MATa/ $\alpha$ , <i>SIZ1/siz1<math>\Delta</math>::HygB, cir<sup>0</sup></i>  |
| YAC186             | MATa/ $\alpha$ , <i>MMS21/mms21-sp::URA3, lys2<math>\Delta</math>, MET15, cir<sup>0</sup></i>  |
| YAC188             | MATa/ $\alpha$ , <i>SIZ1/siz1<math>\Delta</math>::HygB, SIZ2/siz2<math>\Delta</math>::HIS3, cir<sup>0</sup></i>  |
| YAC203             | YAC188 <i>TLC1/tlc1<math>\Delta</math>::LEU2, MMS21/mms21-sp::URA3</i>   |
| YAC219             | MATa/ $\alpha$ , <i>TLC1/tlc1<math>\Delta</math>::LEU2, MMS21/mms21-sp::URA3, YKU70/yku70<math>\Delta</math>::HIS3, cir<sup>0</sup></i>  |
| YAC247             | MATa/ $\alpha$ , <i>MMS21/mms21-sp::URA3, SGS1/sgs1<math>\Delta</math>::HIS3, CDC13/cdc13-1, cir<sup>0</sup></i>   |
| YAC306             | MATa, <i>smc6-9-3HA::HIS3</i>  |
| YAC307             | MATa, <i>smc6-9-3HA::HIS3</i>  |
| YAC308             | MATa, <i>smc6-9-3HA::HIS3, MMS21/mms21-sp::URA3</i>  |
| YAC311             | MATa, <i>smc5-6-3HA::HIS3</i>  |
| YAC312             | MATa, <i>smc5-6-3HA::HIS3</i>  |
| YAC313             | MATa, <i>smc5-6-3HA::HIS3, MMS21/mms21-sp::URA3</i>  |
| Y8205 <sup>0</sup> | MATa, <i>can1<math>\Delta</math>::STE2pr:Sp-his5, lyp1<math>\Delta</math>::STE3pr:LEU2, his3<math>\Delta</math>1 leu2<math>\Delta</math>0 ura3<math>\Delta</math>0</i>   |
| YAC317             | MATa, <i>mms21-sp::URA3, lyp1<math>\Delta</math>::STE3pr:LEU2, his3<math>\Delta</math>1 leu2<math>\Delta</math>0 ura3<math>\Delta</math>0</i>  |
| YAC328             | YAC203 <i>SMC5/SMC5-TAP::spHIS5</i>  |
| YAC357             | Y8205 <i>smt3<math>\Delta</math>::KanMX, pAG416-GPDp-YFP-SMT3</i>  |

YAC389 MAT $\alpha$ , *siz1* $\Delta$ ::*HygB*, *lyp1* $\Delta$ ::*STE3pr:LEU2*, *his3* $\Delta$ 1 *leu2* $\Delta$ 0 *ura3* $\Delta$ 0

YAC390 MAT $\alpha$ , *siz2* $\Delta$ ::*KanMX*, *lyp1* $\Delta$ ::*STE3pr:LEU2*, *his3* $\Delta$ 1 *leu2* $\Delta$ 0 *ura3* $\Delta$ 0

YAC391 MAT $\alpha$ , *siz1* $\Delta$ ::*HygB*, *siz2* $\Delta$ ::*KanMX*, *lyp1* $\Delta$ ::*STE3pr:LEU2*, *his3* $\Delta$ 1 *leu2* $\Delta$ 0 *ura3* $\Delta$ 0

YAC392 MAT $\alpha$ , *mms21-sp*::*URA3*, *siz1* $\Delta$ ::*HygB*, *lyp1* $\Delta$ ::*STE3pr:LEU2*, *his3* $\Delta$ 1 *leu2* $\Delta$ 0 *ura3* $\Delta$ 0

YAC393 MAT $\alpha$ , *mms21-sp*::*URA3*, *siz2* $\Delta$ ::*KanMX*, *lyp1* $\Delta$ ::*STE3pr:LEU2*, *his3* $\Delta$ 1 *leu2* $\Delta$ 0 *ura3* $\Delta$ 0

YAC399 Y8205 *mms21-sp*::*URA3*

YAC410 Y8205 *smc5-6-3HA*::*HIS3*

YAC411 Y8205 *smc6-9-3HA*::*HIS3*

YAC484 MAT $\alpha$ , *tlc1* $\Delta$ ::*spHIS5*

YAC749 MAT $\alpha$ ,  $\Delta$ ::*HYG*, pRS316::*uba2-ts10*

YAC755 MAT $\alpha$ , *smc6-9-HA*::*HIS3*, *uba2* $\Delta$ ::*HygB*, pRS316-*uba2-ts10*

YAC757 MAT $\alpha$ , *smc5-6-HA*::*HIS3*, *uba2* $\Delta$ ::*HygB*, pRS316-*uba2-ts10*

YAC768 MAT $\alpha$ / $\alpha$ , *SMC5/smc5-6-3HA*::*HIS3*, *TLC1/tlc1* $\Delta$  *cir*<sup>0</sup>

YAC769 MAT $\alpha$ / $\alpha$ , *SMC6/smc6-9-3HA*::*HIS3*, *TLC1/tlc1* $\Delta$  *cir*<sup>0</sup>

YAC873 MAT $\alpha$ , *smc5-6-3HA*::*HIS3*, *siz1* $\Delta$ ::*HYG*

YAC874 MAT $\alpha$ , *smc5-6-3HA*::*HIS3*, *siz2* $\Delta$ ::*LEU2*

YAC877 MAT $\alpha$ , *smc6-9-3HA*::*HIS3*, *siz1* $\Delta$ ::*HYG*

YAC879 MAT $\alpha$ , *smc6-9-3HA*::*HIS3*, *siz2* $\Delta$ ::*LEU2*

Y500<sup>&</sup> MAT $\alpha$ , *smc5* $\Delta$ ::*KanMX* [pGC251-*LEU2 smc5-3I*]

\*Torres-Rosell J, Machin F, Farmer S, Jarmuz A, Eydmann T, Dalgaard JZ, Aragon L (2005) *SMC5 and SMC6 genes are required for the segregation of repetitive chromosome regions. Nat Cell Biol* 7(4): 412-419

<sup>Φ</sup>Tong, A. H. Y., Boone, C., Ian, S., and Michael, J. R. S. (2007) 16 High-Throughput Strain Construction and Systematic Synthetic Lethal Screening in. In. *Methods in Microbiology*, Academic Press

<sup>&</sup>Pike, B. L., and Heierhorst, J. (2007) *Mdt1 facilitates efficient repair of blocked DNA double-strand breaks and recombinational maintenance of telomeres. Mol Cell Biol* 27: 6532-6545

